

---

Theses and Dissertations

---

Summer 1951

## The Development of the Turbulent Boundary Layer on Steep Slopes

William John Bauer  
*State University of Iowa*

Follow this and additional works at: <https://ir.uiowa.edu/etd>



Part of the [Aerodynamics and Fluid Mechanics Commons](#)

No known copyright restrictions.

This dissertation is available at Iowa Research Online: <https://ir.uiowa.edu/etd/5369>

---

### Recommended Citation

Bauer, William John. "The Development of the Turbulent Boundary Layer on Steep Slopes." PhD (Doctor of Philosophy) thesis, University of Iowa, 1951.

<https://doi.org/10.17077/etd.b9f2xp9n>

---

Follow this and additional works at: <https://ir.uiowa.edu/etd>



Part of the [Aerodynamics and Fluid Mechanics Commons](#)

THE DEVELOPMENT OF THE TURBULENT BOUNDARY LAYER ON STEEP SLOPES

by

William John Bauer

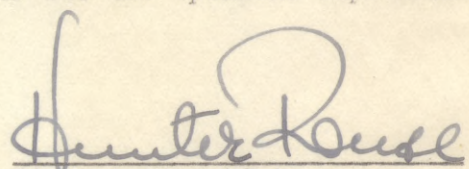
A dissertation submitted in partial fulfillment of the requirements for the degree of Doctor of Philosophy, in the Department of Mechanics and Hydraulics, in the Graduate College of the State University of Iowa

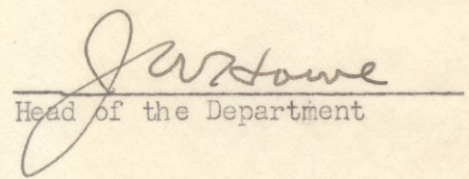
August, 1951

STATE UNIVERSITY  
OF IOWA  
LIBRARY

11951  
B344  
cop. 2

This dissertation is hereby approved as a credit-  
able report on an engineering project or research carried out  
and presented in a manner which warrants its acceptance as a  
prerequisite for the degree for which it is submitted. It is  
to be understood, however, that neither the Department of  
Mechanics and Hydraulics nor the dissertation advisor is res-  
ponsible for the statements made or for the opinions expressed.

  
Dissertation Advisor

  
Head of the Department

#### ACKNOWLEDGMENTS

This project was sponsored by the Waterways Experiment Station of the Corps of Engineers under contract DA-22-079-eng-9 with the Iowa Institute of Hydraulic Research. The author appreciates the advice and criticism contributed by Dr. Hunter Rouse, Director of the Institute, under whose direction the investigation was made. In many phases of the work other members of the Institute staff rendered their experienced help and suggestions to the benefit of the project. To them also, the writer expresses his thanks.

## TABLE OF CONTENTS

	Page
INTRODUCTION . . . . .	1
BACKGROUND OF THE PROBLEM . . . . .	2
Theory of the Boundary Layer Applied to Steep Slopes . . . . .	2
Definitions of Boundary-layer Length Parameters . . . . .	4
The von Kármán Momentum Equation . . . . .	6
The Kármán-Prandtl Velocity-Distribution Equations . . . . .	7
Related Investigations . . . . .	7
EXPERIMENTAL ASPECTS . . . . .	12
Equipment . . . . .	12
Data . . . . .	19
ANALYSIS OF THE DATA . . . . .	23
Dynamic Analysis . . . . .	23
Dimensional Analysis . . . . .	26
Analytical Techniques . . . . .	27
Dimensional Plots . . . . .	29
Dimensionless Plots . . . . .	30
DISCUSSION OF THE RESULTS . . . . .	33
The Role of the Discharge . . . . .	33
The Role of the Slope . . . . .	34
The Role of the Boundary Roughness . . . . .	34
The Nominal Thickness of the Boundary Layer . . . . .	36
The Shape of the Velocity Profile . . . . .	38
The Coefficient of Boundary Shear for the Glass . . . . .	39
The Coefficient of Boundary Shear for the Screen . . . . .	39
APPLICATION TO THE DESIGN PROBLEM . . . . .	42
Outline of the Method of Approach . . . . .	42
Illustrative Example . . . . .	42
CONCLUSIONS . . . . .	45
REFERENCES . . . . .	47

TABLE OF FIGURES

Figure	Page
1. Definitions of $\delta$ , $\delta^*$ , and $\theta$ . . . . .	48
2. Steep Flume . . . . .	49
3. General Views of the Flume . . . . .	50
4. General Views of the Crests . . . . .	51
5. Stilling Tank Details . . . . .	52
6. Stagnation Tubes . . . . .	53
7. Maximum Discharge on the 20° Slope . . . . .	54
8. Maximum Discharge on the 40° Slope . . . . .	54
9. Maximum Discharge on the 60° Slope . . . . .	55
10. Velocity Profiles, Glass Boundary, 20° Slope, 2.98 cfs/ft. .	56
11. Velocity Profiles, Glass Boundary, 40° Slope, 3.68 cfs/ft. .	57
12. Velocity Profiles, Glass Boundary, 60° Slope, 3.65 cfs/ft. .	58
13. Velocity Profiles, Screen Boundary, 20° Slope, 2.98 cfs/ft .	59
14. Velocity Profiles, Screen Boundary, 40° Slope, 3.68 cfs/ft .	60
15. Velocity Profiles, Screen Boundary, 60° Slope, 3.65 cfs/ft .	61
16. Velocity Profiles, Glass Boundary, 40° Slope, 3.68 cfs/ft. .	62
17. Velocity Profiles, Screen Boundary, 60° Slope, 3.65 cfs/ft .	63
18. Water Surface, Screen Boundary, 20° Slope, (a) 1.22 cfs/ft .	64
(b) 2.98 cfs/ft .	65
19. Definition Sketch for Application of Momentum Principle. . .	66
20. Nominal Thickness of the Boundary Layer . . . . .	67

TABLE OF FIGURES

(continued)

Figure	Page
21. Displacement and Momentum Thicknesses, 20° Slope . . . . .	68
22. Displacement and Momentum Thicknesses, 40° Slope . . . . .	69
23. Displacement and Momentum Thicknesses, 60° Slope . . . . .	70
24. $\delta/x = f_1( Ux/\nu , k/x , S , q )$ . . . . .	71
25. $\delta/x$ as a Function of $x/k$ . . . . .	72
26. $c_f$ as a Function of $R_\delta , k , S$ . . . . .	73
27. $c_f$ as a Function of $\delta/k$ . . . . .	74
28. $H$ as a Function of $R , S$ . . . . .	75
29. $H$ as a Function of $x/k , S$ . . . . .	75
30. Graphical Solution of Illustrative Example . . . . .	76

## TABLE OF SYMBOLS

A	=	a constant
B	=	a constant
b	=	a constant
C	=	a constant
$c_f$	=	$\tau_0 / \rho U^2 / 2$ = local coefficient of boundary shear
f	=	$4\tau_0 / \rho V^2 / 2$ = Darcy-Weisbach resistance coefficient
g	=	acceleration of gravity = 32.2 feet/second <sup>2</sup>
H	=	shape parameter of the velocity profile
k	=	equivalent Nikuradse roughness height
m	=	a constant
n	=	the exponent in $u = m y^n$
p	=	pressure at a point
q	=	discharge per foot of spillway width
S	=	slope of the boundary (sine of the angle from the horizontal)
U	=	velocity of the potential flow
u	=	velocity at a point within the boundary layer
V	=	average velocity across a section
x	=	distance in the direction of flow = $U^2 / 2gS$
y	=	normal distance from the boundary
$y_0$	=	total thickness of the flow measured normal to the boundary



## TABLE OF SYMBOLS

- $\gamma$  = unit weight of the fluid
- $\delta$  = nominal thickness of the boundary layer
- $\delta^*$  = displacement thickness of the boundary layer
- $\eta$  = the shape parameter of Gruschwitz
- $\theta$  = momentum thickness of the boundary layer
- $\mu$  = dynamic viscosity of the fluid
- $\nu$  = kinematic viscosity of the fluid
- $\rho$  = mass density of the fluid
- $\tau_0$  = shear stress at the boundary

## INTRODUCTION

The problem considered herein arose first from the desire to locate the upstream limit of air entrainment in spillway flows. Since air entrainment is possible only if the free surface is turbulent, and since the usual source of that turbulence is the turbulent boundary layer, the present investigation arose as a logical approach to the problem.

More specifically, the problem requires the formulation of a basis for the design calculation of the location at which the free surface first becomes turbulent due to the proximity of the turbulent boundary layer. From this point downstream, air entrainment produces a bulking of the flow which requires that flanking walls be constructed much higher than necessary to confine flow at potential or near potential depth. Certain knowledge of the absence of air entrainment upstream from a certain point permits the elimination of these extra high walls in that region, effecting an important saving in cost. The problem of air entrainment itself is being handled as a separate project at the St. Anthony Falls Hydraulic Laboratory, University of Minnesota.

The results of this investigation may also be added to the accumulating store of knowledge concerned with turbulent boundary layers in general. To this end the data will be analyzed according to conventional definitions and compared with the results of other boundary-layer investigations.

## BACKGROUND OF THE PROBLEM

Theory of the Boundary Layer Applied to Steep Slopes

The assumption of a non-viscous fluid yields a solution to the problem of flow down steep slopes which has long since taken its place in engineering literature. By application of the requirements of irrotationality and of the principles of conservation of energy and matter, together with the condition that the pressure be constant along the free surface, one determines the velocity, the pressure, and the location of the free surface at any station along the slope. Curvilinear geometry makes the analysis more tedious but offers no fundamental difficulty.

When viscosity enters the problem, however, one employs the expedient of separating the flow into two domains, as suggested by Prandtl [1] in his original enunciation of the boundary-layer concept. Prandtl considered that in many flow situations (particularly those involving fluids of low viscosity of which water is a good example), the viscous effects were largely confined within a relatively narrow zone adjacent to the boundary, so that the greater part of the flow behaved very nearly as if the fluid were non-viscous. He then proposed that these two domains be treated separately. The domain of large viscous effects is called the boundary layer; the domain of negligible viscous effects is called herein the zone of near-potential flow, indicating that it is slightly different from the potential flow of the non-viscous fluid. On the spillway both domains exist contiguously,

the near-potential dominating the picture at the beginning and the boundary layer comprising nearly the entire depth of flow at its downstream limit of development.

Flow in the near-potential domain remains essentially irrotational and free from shear forces. Aside from the displacement in the direction away from the boundary, flow in this domain is handled as if one were dealing with the spillway flow of a non-viscous fluid. This displacement is never large enough in a spillway problem to produce a significant difference between the magnitude of the actual velocity in the near-potential domain and that computed at the same station on the basis of irrotational flow. The displacement is significant in determining the depth of flow, however, increasing that quantity beyond the value predicted by irrotational flow theory.

Flow within the boundary layer, on the other hand, is complicated by the presence of rotational flow and an additional force, the shear at the boundary. The nature of these two complications is understood only in the case of laminar flow, in which the well known viscous shear relationship applies. The development of laminar boundary layers may be handled without resort to experimental measurement. Unfortunately, the transition from laminar to turbulent boundary layer usually occurs within the first few feet, and often within the first few inches, of development, so that the laminar boundary layer constitutes no significant part of the spillway problem.

The development of the turbulent boundary layer is governed by parameters which have customarily been determined by experiment. In like manner, the solution proposed here depends largely upon laboratory observations of the desired parameters, which are then regimented according to the considerations of previous experience with turbulent flows. This empirical approach is the only one available in view of the lack of knowledge of the principles which govern flow with turbulence.

In addition to the location of the critical point ( i.e., the point at which the free surface of the flow first becomes turbulent due to the proximity of the turbulent boundary layer) and the location of the free surface upstream from it, the goal of this study is to delineate the effect of continuous positive acceleration on the standard boundary-layer parameters. This latter goal culminates in a series of functional relationships presented graphically in the section "ANALYSIS OF THE DATA." In order better to understand the nature of these relationships, and in order to comprehend their significance, a brief review of the analytical background of this study is in order.

#### Definitions of Boundary-layer Length Parameters

In the case of turbulent boundary layers, analysis is based largely on experimental evidence, which is regimented according to a commonly accepted set of definitions. One encounters first of all the nominal thickness of the boundary layer, given the symbol  $\delta$  . It is

defined as that distance  $y$  from the boundary at which the magnitude of the velocity is 99% of the value predicted by irrotational flow theory. A graphical presentation of this relationship is shown in Figure 1.

In addition to the nominal thickness, two other length parameters are commonly employed in the study of boundary layers. One of these is the displacement thickness, given the symbol  $\delta^*$ , which is the distance which the potential flow has been displaced from the boundary by the presence of the boundary layer. The other is the momentum thickness, given the symbol  $\theta$ , which is a measure of the defect of momentum flux within the boundary layer. In the symbols of mathematics, these two lengths are defined as follows (for two-dimensional flow):

$$\text{Displacement thickness} \quad \delta^* = \int_0^{\delta} [1 - u/U] dy \quad (1)$$

$$\text{Momentum thickness} \quad \theta = \int_0^{\delta} [u/U - (u/U)^2] dy \quad (2)$$

where  $\delta^*$  is the displacement thickness,

$\theta$  is the momentum thickness,

$\delta$  is the nominal thickness of the boundary layer,

$u$  is the velocity at a point within the boundary layer,

$U$  is the velocity of the potential flow,

and  $y$  is the distance from the boundary,

The significance of these definitions is illustrated in Figure 1.

### The von Kármán Momentum Equation

Using the two length parameters  $\delta^*$  and  $\theta$ , von Kármán [2] has formulated an expression for the boundary shear in accelerating flows:

$$\frac{2\tau_0}{\rho U^2} = c_f = 2 \frac{d\theta}{dx} + (H+2) \frac{\theta}{U^2} \frac{\partial U^2}{\partial x} \quad (3)$$

in which  $c_f$  is the local coefficient of boundary shear,

$\tau_0$  is the intensity of boundary shear,

$\rho$  is the mass density of the fluid,

$x$  is distance in the direction of flow,

and  $H$  is the shape parameter defined as  $\delta^*/\theta$ .

All other symbols are as previously defined. If one knows the functions which relate  $U$ ,  $c_f$ , and  $H$  to  $x$ , one is then able to integrate this expression numerically to obtain  $\theta$  as an explicit function of  $x$ . Of these three functions, the first is given in the usual case, the other two often being assumed according to the notions of boundary layer behavior indicated by related experiments.

Rather than introduce at this point a synthesis of the development of the turbulent boundary layer on steep slopes based upon the numerical integration of Equation (3), the author chooses to reserve this expression for the evaluation of the  $c_f$  function for smooth and rough boundaries in accelerating flows. The results will be compared with the observations of other experimenters. Such comparisons may some day lead to the principles as yet undiscovered which, in combination

with the von Kármán momentum equation, will allow the synthesis of turbulent boundary-layer development without the use of empirical expressions of laboratory data.

### The Kármán-Prandtl Velocity Distribution Equations

Many of the notions about boundary layers find their basis in an abundance of experimental data concerning flow in pipes. Among them are the Kármán-Prandtl velocity-distribution equations for turbulent flow near smooth and rough boundaries, the expressions being given in Rouse [3] in the following form:

$$\frac{u}{\sqrt{\tau_0/\rho}} = 5.75 \text{ LOG}_{10} \frac{\sqrt{\tau_0/\rho} y}{\nu} + 5.5 \quad \text{Smooth (4)}$$

$$\frac{u}{\sqrt{\tau_0/\rho}} = 5.75 \text{ LOG}_{10} y/k + 8.5 \quad \text{Rough (5)}$$

These expressions are derived by von Kármán by application of the Prandtl mixing-length theory, the assumption of a constant shear stress throughout the region, and the neglect of the laminar shear. The experimental data of Nikuradse [4] and others seem to confirm the derivation.

### Related Investigations

Boundary-layer developments on flat plates in uniform flow have been synthesized by mathematical conversion of pipe-flow principles, as well as measured in the laboratory. Schlichting [5], in a lecture series on boundary-layer theory, presents an excellent review of the



conversion techniques as applied to both smooth and rough flat plates. In both cases, the basic assumptions are that the thickness of the boundary layer corresponds to the radius of the pipe and that the shape of the velocity profile in the boundary layer is the same as that in a pipe. Although this last assumption is definitely in error, values of  $c_f$  obtained experimentally agree generally with those predicted by these conversion techniques in the case of the smooth plate.

The development of the boundary layer in non-uniform flow was studied by Gruschwitz [6], who made measurements along the converging and diverging plane walls of a channel. In the development of his method of analysis, Gruschwitz presents the idea that the shape of the velocity profile may be characterized by a single parameter, which he defines as

$$\eta = 1 - (u_\theta/U)^2 \quad (6)$$

in which  $\eta$  is the Gruschwitz shape parameter, and  $u_\theta$  is the velocity at  $y = \theta$ .

With this as a background, he proceeds with a numerical integration of Equation (3) implemented with two empirical expressions. One of these, for  $c_f$ , is obtained by conversion of pipe-flow principles according to the method indicated in the preceding paragraph. The other is for his shape parameter which he obtains by plotting the the experimentally obtained values of  $\eta$  against pressure gradient and the Reynolds number. He noted little dependence upon the Reynolds

number and subsequently eliminated it from consideration in the relation for his shape parameter.

A more recent method for the calculation of boundary-layer developments in flows with pressure gradients is presented by von Doenhoff and Tetervin [7] in a 1943 publication by the National Advisory Committee for Aeronautics. Like Gruschwitz, they consider the velocity profile susceptible of characterization by a single parameter, although they choose to use  $H$  instead of  $\eta$ . In relating  $H$  to the pressure gradient they noted a consistent variation with Reynolds number not discovered by Gruschwitz. This variation was eliminated by expressing  $H$  as a function of the quotient of the non-dimensional pressure gradient and the coefficient of boundary shear. For the determination of this latter quantity they used the Squire-Young formula, which was the result of experiments involving flows with both pressure increase and decrease. In this connection they noted "no systematic variation of the skin-friction coefficient with the shape parameter was indicated by the data."

Within the last year another analysis has been proposed by Tetervin and Lin [8] for the calculation of turbulent boundary layers with pressure gradients. The required relationships from experiment are those between boundary shear and pressure gradient, as well as that between the integral of shearing stresses across the boundary layer and the pressure gradient. These relationships are offered by Granville [9] in a recent publication of the David W. Taylor Model Basin, together

with another excellent summary of analytical approaches to the calculation of the turbulent boundary layer with pressure gradient.

Very recently in France, Halbronn [10] conducted an investigation similar to the one reported herein, although he made no attempt to secure a controlled variation of slope and roughness. Halbronn again uses Equation (3), although in somewhat different form, and taking the velocity distribution and shear relationship to be the same as that in a pipe, he obtains an expression which enables him to determine boundary-layer dimensions. Treating flow outside the boundary layer as non-viscous flow, he is then able to determine the locus of both the free surface and the upper limit of the boundary layer which he projects to an intersection which he calls the "point critique" as we shall continue to do.

Halbronn compared the location of this critical point predicted by his analysis with observations made by him and others both in the laboratory and in the field. All of his experimental measurements were made at values of  $Ux/\nu$  less than  $4 \times 10^6$ , while those of the present investigation were taken over the range  $1.4 \times 10^6$  to  $3.7 \times 10^7$ . Certain observations made by Hickox [11] of the flow on the spillway of Norris Dam at Reynolds numbers in the range  $1.5 \times 10^8$  to  $1.5 \times 10^9$  were also compared to analytical predictions, as well as observations of flow on models of the spillway of Norris Dam and that of Bort-les-Orgues. The agreement was good in all cases.

With this we reach an end to the discussion of the material which forms a background for the present investigation. The author does not presume that he has mentioned here all work significant to the study of the development of the turbulent boundary layer on steep slopes. The intention here is to introduce the subject in a general way to the non-specialist in boundary-layer work, and to furnish suggestions for possible further study of the background. Those who are interested in further reading are referred to the references at the end of this paper, which, although short, nevertheless will in turn provide additional references to the end that a very complete coverage is secured.

## EXPERIMENTAL ASPECTS

Equipment

The approach of the present investigation is made largely from the experimental standpoint. In order to achieve a systematic variation of the quantities involved, laboratory equipment designed expressly for the project was constructed, using funds supplied through a contract between the Iowa Institute of Hydraulic Research and the Waterways Experiment Station of the Corps of Engineers. In simplest terms, this equipment provided for the introduction of non-turbulent flow to the crest of a steep flume of controlled slope and roughness. Dimensions were limited by the amount of space and water economically available, but were regarded as adequate for the determination of information sufficient for design purposes.

The central feature of the equipment is the glass-lined flume, an open channel made in two sections, one 12 feet and the other 4 feet long. As Figure 2 shows, the glass floor is supported on adjustable shoes which provide means of alignment independent of the steel frame. This feature made possible an extremely precise floor which deviated from a true plane by no more than 0.002 inch. The glass floor itself provided the smooth boundary, while a rough boundary was obtained by stretching a piece of screen over it. This screen was 16 x 16 mesh made of bronze wire 0.010 inch in diameter, about which more will be said at another point in this paper. General views of the flume are shown in Figure 3.

Connecting the glass-lined flume with the stilling tank were three spillway crests, one for each of the three slopes used, photographs of which are shown in Figure 4. The profile shape was nearly that of the underside of the nappe of a sharp-crested weir discharging under a 1-foot head. Actually it was made up of an ellipse and a 1.88-power parabola. The vertical semi-axis of the ellipse was 1.51 inches in length, while the horizontal was 3.60 inches. The equation of the parabola was  $y = 0.512 x^{1.88}$ , with  $y$  being measured positively along the horizontal in the direction of flow. The origin of coordinates was the high point of the crest. Brass templates cut to the pattern of these curves were used as screeds in concreting the crests, the mortar being a mixture of Portland cement and sand. The mortar was deliberately left a slight distance below the level of the brass templates and the intervening space filled later with paraffin applied as a liquid. This wax was then shaved with a sharp-cornered straight edge, again using the brass templates as guides, until a smooth and accurate crest profile was achieved.

The center brass template was made thicker than those near the edges of the crests and was drilled at intervals to form a series of piezometric openings, which were connected by flexible tubes to a manometer bank, where the pressure head at each opening was measured. Smooth curves drawn through points plotted from such measurements are shown in Figures 7 through 9 for each of the three slopes of the flume. Fortunately, effects of curvilinear flow are insignificant a short

distance below the crest region so that the assumption of hydrostatic pressure distribution in the direction normal to the boundary is sufficiently accurate on the straight portion of the flume for the purpose of determining the velocity field.

The weir crests were connected at their upstream ends to the stilling tank, the function of which was to deliver non-turbulent, potential-like flow. This type of flow was approached by using a rather large tank equipped with a series of baffles, grids, and screens arranged in circular arcs as shown in Figure 5. Two objectives were achieved by this arrangement; first of all, the presence of a pressure drop across each baffle, grid, and screen produced an effect which distributed the velocity in a potential-like pattern; secondly, the arrangement of coarse to fine gradation of the baffles, grids, and screens reduced the turbulence of the incoming flow to such a small scale that it was effectively dissipated before it reached the weir crests, so that essentially the only turbulence present within the flow on the slope was that engendered by the boundary itself.

Several sizes of stagnation tubes were used to make the stagnation-pressure surveys, but after a little experience with each, two were picked for general use. One was relatively large, being 0.084 inch in diameter, and one relatively small, being 0.021 inch in diameter. Results of the two were compared with a view toward discovering at what distance from the boundary agreement between them began. This point was reached when the centerline of the large tube was about one diameter

from the boundary. The advantage of the large tube was that it permitted the taking of readings in rapid succession, since the smaller tube had such a high resistance to flow that considerable time elapsed before equilibrium was attained in a new position. On the other hand, this high resistance to flow completely damped out all oscillations of the level of the mercury in the open manometer, permitting more precise readings, so that the smaller tube was used as a general rule. The fluctuations of the level of the mercury in the open manometer associated with the use of the large tube were very evident as long as it was located within the boundary layer, and disappeared completely when the tube was moved to the non-turbulent zone outside the boundary layer. The line between the two domains was determinable with surprising precision on the basis of the presence and absence of the fluctuations, although it was always outside the locus of  $y = \delta$  by about a diameter of the tube. The drawings of the stagnation tubes are presented in Figure 6.

The mounting of the stagnation tubes was such that their motion was normal to the boundary. In order to determine the precise location of the tube with respect to the boundary, an Ames dial graduated to 0.001 inch was connected directly to the stagnation-tube support. The origin of the  $y$  coordinate was determined in two ways. The first was simply visual, the tube being viewed in the direction normal to its long axis with the eye slightly above the place of the glass floor, so that both the tube and its reflection were seen simultaneously. The tube



was carefully lowered until the tube and its image made contact, at which point the reading of the Ames dial was taken. The process was repeated and the second reading compared with the first. With great care, one could duplicate readings within 0.001 inch. The value of  $y$  was taken to be one-half the outside diameter of the stagnation tube when it was in this position of initial contact. The second method employed a metal shim of known thickness placed between the glass and the tube. Upon initial contact an electrical circuit was completed. In this position the value of  $y$  was taken to be one-half the outside diameter of the tube plus the thickness of the shim. Since the visual method could be used under water, and since it agreed with the second method within 0.001 inch, it was employed almost exclusively for all work done on the glass boundary.

The value of the  $y$  coordinate for all runs made with the screen boundary was measured from the mid-plane of the screen to the centerline of the tube. The origin of coordinates was determined in this case by measuring the distance between the lowest extremity of the stagnation tube and the flat surface forming the bottom of the support tube. The tube was then lowered to firm contact between the screen and this flat surface, and then raised the known distance between the lowest extremity of the tube and this flat surface. In this position the value of the  $y$  coordinate was taken to be one-half the outside diameter of the stagnation tube plus one diameter of the wire from which the screen was made.

The stagnation tubes were attached to a movable carriage which traveled the length of the flume, and upon which the open mercury manometer was mounted. Vertical alignment of the manometer was maintained by re-setting it for each slope. Using a gage graduated to 0.01 foot and equipped with a vernier, the steady level of the mercury could easily be determined within 0.001 foot. The ratio between the area of the mercury tube and that of the mercury-water well was such that one multiplied the number of observed feet of mercury by 13.85 in order to obtain the corresponding number of feet of water. The level of the mercury which corresponded to a zero stagnation pressure was determined by noting that the stagnation pressure observed in the domain outside the boundary layer must correspond to the original total head.

One series of runs was made with the glass boundary and a second with a boundary formed by stretching a length of screen over the floor of the flume. The screen was 16 x 16 mesh made of 0.010-inch-diameter bronze wire. It was chosen because it was uniform, easily reproducible, convenient to apply and remove, and very low in cost. It was important to use a piece of screen completely free from folds, bulges, and kinks; only a perfect piece would lie flat on the glass without the use of an adhesive. For this reason, the material used was taken from a previously unopened roll. Both ends were soldered to brass bars, one of which was screwed to the vertical wall of the stilling tank about three feet below the crest. The other was first fastened to the

downstream end of the flume in such a manner that the screen could be stretched. Later it was found that the combination of gravity and shear forces on the screen produced adequate stretching, so that fastening to the lower end of the flume was eliminated. This made very rapid removal and application of the screen possible. In order to avoid damaging the mesh in handling, a wood drum of special design was employed.

In order to determine the effective roughness, a piece of screen from the same roll was applied to the floor of one of the flumes of the Iowa Institute of Hydraulic Research. Because the floor of the flume was not as plane as was the glass floor of the steep flume (although the deviation from a true plane was in the form of a smooth curve about 20 feet long, the low point of which was about 1 mm. from a straight line drawn between the ends of the curve), it was necessary to use an adhesive to secure the screen to the floor at all points. The maximum thickness of this adhesive film was on the order of 0.004 inch. Uniform flow was established over the screen, uniformity being determined by both depth measurements and stagnation-tube surveys. Discharge was measured by an orifice meter located in the pipe line supplying the flume. Knowing the discharge, the depth, and the slope, one could compute the values of  $f$ ,  $k$ , and  $n$ , as tabulated at this point. The equations used to determine  $f$  and  $n$  are the ordinary Darcy-Weisbach and Manning expressions, respectively, while that used to determine  $k$  comes from an application of the Karman-Prandtl

velocity distribution law to the case of two-dimensional flow, as given in Rouse [3]:

$$1/\sqrt{f} = 2.06 \log_{10} y_0/k + 2.11 \quad (7)$$

Run	Slope	Depth	Average Velocity	f	k	n
1	0.0167	0.286 ft.	5.58 ft./sec.	0.0394	0.0097 ft.	0.0150
2	0.0100	0.286 ft.	4.47 ft./sec.	0.0368	0.0079 ft.	0.0146
3	0.0100	0.086 ft.	1.89 ft./sec.	0.0620	0.0096 ft.	0.0155
4	0.0167	0.070 ft.	2.21 ft./sec.	0.0655	0.0090 ft.	0.0145

Note that the values of k and n indicate a roughness comparable to rough concrete. Thus, in the remainder of this paper, the development of the boundary layer over the 16x16 mesh screen will be considered a good approximation to that occurring over rough concrete.

### Data

The experimental data were obtained from stagnation-pressure surveys made in flows down each of the three slopes, with variations in the roughness of the boundary and in the rates of flow. Water surface profiles for the highest rates of flow used on each of the three slopes are shown in Figures 7 through 9. (Note that the values of pressure head are plotted vertically in Figures 7 through 9; the dashed line is drawn approaching the limit of  $y_0 \sec \alpha$  on the straight portion of the flume.) From the curvature of the water surface one may make an

estimate of the pressure distribution existing within the flow and compare it with the hydrostatic distribution in the direction normal to the boundary which was assumed in this analysis. The greatest curvature of a region from which data included in this analysis were obtained is between Stations 3 and 4 on the  $20^{\circ}$  slope. It is significant to note that in this region the assumption of a hydrostatic distribution of pressure in the direction normal to the boundary introduces an error in the magnitude of the velocity on the order of 1%. The error at stations further down the slope is much less, so that they are neglected in the computations for the velocity.

In making the stagnation-pressure surveys the carriage was located at a fixed position on the flume and a normal traverse made. After making 10 to 30 stagnation-pressure measurements at different distances from the boundary, the carriage was moved to the next station and the process repeated. The result was a characterization of the stagnation-pressure field by knowledge of its magnitude at many discrete points, these values being presented in terms of the velocity distribution which they indicated. Velocity profiles obtained from the six runs made with the highest rates of discharge are presented graphically in Figures 10 through 15. Note that these six plots are in the form of logarithm of velocity as a function of logarithm of the distance from the boundary. Two others are presented in Figures 16 and 17, which are plotted in the form of velocity as a function of logarithm of the distance from the boundary. No velocity profiles are presented

which resulted from surveys made at the lower rates of discharge, although data deduced from them are included in Figures 20, 24, and 25.

In addition to the stagnation-pressure survey, certain other observations were made by visual inspection of the external and internal appearance of the flow. One noted first of all that the effect of the walls of the flume is to produce small waves which issue normal to the wall. Being superimposed upon the general downstream motion of the water, the waves have a total velocity which is the vector sum of the celerity and the surface velocity of the fluid over which the wave is being propagated. Since the celerity of the wave is decreasing while that of the fluid as a whole is increasing, the motion of the wave is along a curve of such a shape that a region in the form of an inverted cusp in the central portion of the flow is largely unaffected by the presence of side boundaries.

One also observed that the free surface in the neighborhood of the critical point was characterized by a change over a relatively short distance from a smooth, glass-like, transparent appearance to one which was rough and nearly opaque. Figure 18 illustrates this transition photographically, with pictures taken with the aid of a stroboscopic light flash of  $1/5000$  second duration. The apparent location of this transition was noted and compared later to the location of the critical point determined graphically. Comparison showed that slight disturbances occur upstream from the critical point, probably due to the fact

that there is a turbulent region outside the boundary layer if one takes the empirical definition for the boundary layer thickness used here, corresponding to  $u/U \approx 0.99$  . However, the effect intensifies rapidly from this point of initial disturbance on, and reaches a well developed stage at the critical point.

Careful measurement showed that energy loss in the domain outside the boundary layer is practically non-existent. The author connected a flexible translucent tube completely filled with water to the stagnation tube when it was located in flow outside the boundary layer at the greatest possible distance from the stilling tank. The water level in this translucent tube rose to a distance above the water in the stilling tank which was equal to the computed value of the velocity head at the point of comparison. If there was any energy loss, its magnitude was less than 0.001 foot in a region where the velocity head was on the order of 10 feet.

No further comment on the data will be made at this point, additional aspects being reserved for presentation in the section "DISCUSSION OF THE RESULTS."

## ANALYSIS OF THE DATA

Dynamic Analysis

Since the von Kármán momentum equation forms the sole basis for the dynamic analysis of the turbulent boundary layer, it is significant to review its derivation. One starts with a graphical representation of the flow within the boundary layer as shown in Figure 19, and evaluates the net change in momentum flux as the fluid passes through an elementary volume such as the one labeled ABCD. The net change in momentum flux in the  $x$  direction is equated to the algebraic summation of all the forces in the  $x$  direction which act on this same elementary volume of fluid. Borrowing a technique used by Schlichting, the calculation is performed with the aid of the following table:

Section	Flow Out	Momentum Flux Out
AB	$-\int_0^h \left[ u - \frac{\partial u}{\partial x} \frac{dx}{2} \right] dy$	$-\rho \int_0^h \left[ u - \frac{\partial u}{\partial x} \frac{dx}{2} \right]^2 dy$
CD	$\int_0^h \left[ u + \frac{\partial u}{\partial x} \frac{dx}{2} \right] dy$	$\rho \int_0^h \left[ u + \frac{\partial u}{\partial x} \frac{dx}{2} \right]^2 dy$
BC	$-\int_0^h \frac{\partial u}{\partial x} dx dy$	$-\rho \int_0^h U \frac{\partial u}{\partial x} dx dy$
$\Sigma F_x$	0	$\rho \int_0^h \left[ 2u \frac{\partial u}{\partial x} dx - U \frac{\partial u}{\partial x} dx \right] dy$

The summation of the momentum flux is next changed in form in order to introduce  $\delta^*$  and  $\theta$  as ordinarily defined. This results in an



expression of the form

$$\frac{\Sigma F_x}{\rho U^2 dx} = \int_0^h \frac{\partial}{\partial x} \left[ \left( \frac{u}{U} \right)^2 - \frac{u}{U} \right] dy - \frac{1}{U} \frac{\partial U}{\partial x} \int_0^h \left[ \frac{u}{U} - \left( \frac{u}{U} \right)^2 \right] dy + \frac{1}{U} \frac{\partial U}{\partial x} \int_0^h \left( \frac{u}{U} \right)^2 dy \quad (8)$$

The integrals which thus arise from this application of the principle of conservation of momentum are readily simplified by using the standard definitions of  $\delta^*$  and  $\theta$ . Since the integrand of the first integral vanishes at  $y = \delta$ , one may both change the upper limit of integration from  $h$  to  $\delta$  and remove the differentiation with respect to  $x$  outside the integral. Changing the upper limit of integration on the other integrals as well, and recognizing all three in terms of the ordinary expressions for  $\delta^*$  and  $\theta$ , we have the following simplification:

$$\begin{aligned} \frac{\Sigma F_x}{\rho U^2 dx} &= - \frac{\partial \theta}{\partial x} - \frac{1}{U} \frac{\partial U}{\partial x} \theta + \frac{1}{U} \frac{\partial U}{\partial x} [\delta - \theta - \delta^*] \\ &= - \frac{\partial \theta}{\partial x} - \frac{1}{U} \frac{\partial U}{\partial x} [2\theta + \delta^*] + \frac{\delta}{U} \frac{\partial U}{\partial x} \end{aligned} \quad (9)$$

Turning next to the evaluation of the forces acting on this element of fluid, we note but three: the shear force at the boundary, which may be expressed in terms of the coefficient of boundary shear; the gravitational force, which may be expressed in terms of the acceleration outside the boundary layer; and the pressure gradient force, which may be expressed in terms of the slope of the water surface with

respect to the boundary,  $dy_0/dx$ . The summation of forces acting in the  $x$  direction then becomes

$$\Sigma F_x = -c_f \frac{\rho U^2}{2} dx + \rho \delta U \frac{\partial U}{\partial x} dx + \gamma \sin \alpha \delta \frac{dy_0}{dx} dx \quad (10)$$

Writing the last term with  $\gamma$  expressed as the product  $\rho g$ , and combining it with the gravitational term, we have upon factoring

$$\rho \delta dx \left[ U \frac{\partial U}{\partial x} + g \sin \alpha \frac{dy_0}{dx} \right] \quad (11)$$

One will note that the first term in the parenthesis is an acceleration with a magnitude of  $Sg$ , where  $S$  is the slope of the boundary, while the second term is an acceleration of the magnitude  $(\sin \alpha dy_0/dx g)$ . Since  $dy_0/dx$  is at most 4% and usually less than 1% of  $S$ , it will be dropped from the expression. With this deletion, we have the following upon equating the net change in momentum flux to the summation of forces acting on the elementary volume of fluid:

$$-\frac{d\theta}{dx} - \frac{1}{U} \frac{\partial U}{\partial x} [2\theta + \delta^*] + \frac{\delta}{U} \frac{\partial U}{\partial x} = -\frac{c_f}{2} + \frac{\delta}{U} \frac{\partial U}{\partial x} \quad (12)$$

which simplifies to

$$c_f = 2 \frac{d\theta}{dx} + 2 \frac{\theta}{x} + \frac{\delta^*}{x} \quad (13)$$

This was the equation which was used to evaluate  $c_f$ .

### Dimensional Analysis

A dimensional analysis serves to elucidate the essential variables in the problem and provides the basis for graphical presentation of results. Noting that the viscosity, density, and unit weight of the fluid enter the problem, one may form the following relationships:

$$\delta = f_1(U, x, k, \mu, \rho, g, q, S) \quad (14)$$

$$c_f = f_2(U, x, k, \mu, \rho, g, q, S) \quad (15)$$

$$H = f_3(U, x, k, \mu, \rho, g, q, S) \quad (16)$$

in which  $\delta$  is the nominal thickness of the boundary layer,  
 $U$  is the potential velocity,  
 $g$  is the acceleration of gravity,  
 $x$  is distance in the direction of flow,  $U^2/2gS$ ,  
 $\mu$  is the dynamic viscosity of the fluid,  
 $\rho$  is the mass density of the fluid,  
 $k$  is the equivalent Nikuradse roughness,  
 $q$  is the discharge per foot,  
 $H$  is the shape parameter of the velocity profile,  
 $c_f$  is the coefficient of boundary shear,  
 and  $S$  is the slope of the boundary.

Dimensionless combinations of these variables may be formed as follows:

$$\delta/x = \phi_1 (Ux/\nu, k/x, U^2/gx, q/Ux, S) \quad (17)$$

$$c_f = \phi_2 (Ux/\nu, k/x, U^2/gx, q/Ux, S) \quad (18)$$

$$H = \phi_3 (Ux/\nu, k/x, U^2/gx, q/Ux, S) \quad (19)$$

One will note from the definition of  $x$  that  $U^2/gx$  is directly proportional to the slope of the boundary, so that in general the three independent variables listed above are functions of the Reynolds number, the relative roughness, the slope, and the ratio of the potential depth to  $x$ , the last being an interpretation of the dimensionless expression of the discharge. In the expressions for  $c_f$  and  $H$  one may introduce  $\delta$  for  $x$  without changing the validity of the procedure. The result is that the Reynolds number and the relative roughness are written in terms of the boundary-layer thickness. This furnishes immediately a basis for comparison with uniform flow in pipes or open channels. If the  $x$  is retained, one obtains plots similar to those obtained from research on flat plates in uniform flow.

### Analytical Techniques

In the reduction of the data, the author employed the standard definitions of  $\delta^*$  and  $\theta$ . The actual process by which these values were obtained was one of numerical integration in which the trapezoidal

rule was employed in general. An exception occurs only in treating the region immediately adjacent to the boundary in which no stagnation-pressure measurements were physically possible. Here an assumption was made which was roughly equivalent to extrapolation of the velocity profile according to a function of the form  $u = m y^n$ . A typical value of the exponent  $n$  is  $1/7$ . Integration of the function in the  $y$  direction with this value yields the very simple result that the discharge between  $y = 0$  and  $y = y_1$  is seven-eighths of the product  $u_1 y_1$ . This rule was applied to the numerical integration of the velocity and a similar one for the numerical integration of the velocity squared only in the narrow layer between the boundary and the location of the first stagnation pressure measurement. Since this part of the flow is ordinarily a small part of the whole, inaccuracies made in the estimate of its magnitude have little influence on the final result.

A graphical method was used to determine  $\delta$ . The method consisted simply of extrapolating the straight-line portion of the log-log plot of the velocity profile to its intersection with the line  $u = U$ . The value of  $y$  at this intersection was taken to be the value of  $\delta$ . This method is less dependent upon the judgment of the human eye than is the method of reading from a somewhat arbitrary curve the value of  $y$  at which  $u/U = 0.99$ . It also gives results that correspond to the definition of  $\delta$ , however, at worst within the limits of experimental variation.

The magnitude of the potential velocity  $U$  was determined by equating the vertical distance between the water surface and the line of total head to  $U^2/2g$ . The slight difference between the location of the actual surface and that of the potential flow is insignificant in making this computation, since the effect upon  $U$  is a change in magnitude of about 0.05%.

The same definition for  $x$  is used as that made at the outset of this paper,  $x = U^2/2gS$ , being the one which allows a simplification of Equation (3) to the form of Equation (14)<sup>13?</sup>. This involves an approximation, since the origin of coordinates moves a short distance upstream as one proceeds in the direction of flow, and since the differentiation in the term  $d\theta/dx$  is made with respect to an  $x$  with a fixed origin. Here again, the order of magnitude of the error introduced by this approximation is insignificant, producing at worst a 4% discrepancy in the value of  $c_f$ . Errors of this order of magnitude are associated only with the stations near the crest of the flume. Over by far the greatest part of the flume the error is not detectable.

#### Dimensional Plots

The results of the analysis of the velocity profile are presented first of all in dimensional form so that the reader may have a graphic impression of the data being considered here. In Figure 20  $\delta$  is plotted as a function of  $x$ , the points resulting from tests with both glass and screen boundaries, with all three slopes, and with

various rates of discharge. All of the points plotted here are presented again in dimensionless form in Figure 24.

In Figures 21, 22, and 23 are presented the results of the numerical integrations of the functions which define  $\delta^*$  and  $\theta$ . Smooth curves have been drawn through each series of points. The value of the variable read from these curves was used in the computation of  $c_f$  according to Equation (13), as well as in the determination of  $H$  according to the definition of that quantity.

#### Dimensionless Plots

Figure 24 presents  $\delta/x$  as a function of the Reynolds number, the results obtained from different slopes, from different boundaries, and from different discharges being plotted on the same field. In addition to the observations of this investigation, those of Halbronn and Hickox are also plotted in this figure. Neither Halbronn nor Hickox presented data in the form plotted, so that it was necessary for the author to deduce it from the information they did present. In the case of Halbronn's work, the value of  $\delta$  was obtained from the velocity profile by the same method applied to the data of this investigation. In the case of the observations made by Hickox on the spillway of Norris Dam, the thickness of the boundary layer was taken to be  $\delta^*$  plus the depth of the potential flow at the same discharge and at the same station on the slope.

Figure 25 shows  $\delta/x$  as a function of relative roughness, with results obtained from different slopes and different discharges

being plotted on the same field. Again the observations of Hickox are plotted, with an assumption that the  $k$  of the concrete on the spillway of Norris Dam was 0.005 foot, corresponding to an average concrete surface texture. The value of  $k$  for the screen was taken to be 0.009 foot, according to the results of tests listed on page 19.

Figure 26 shows the  $c_f$  function for both smooth and rough boundaries as a function of the Reynolds number. The value of  $c_f$  was computed by application of Equation (13) to the data obtained from the smooth curves drawn in Figures 21, 22, and 23. Also plotted in Figure 26 is a smooth curve labeled

$$1/\sqrt{c_f} = 4.06 \log_{10} \sqrt{c_f} R_s + 3.28 \quad (20)$$

This equation was obtained by substituting in Equation (4) the point  $y = \delta$ ,  $u = U$ , and also expressing the boundary shear in terms of  $c_f$ .

Figure 27 is the counterpart of Figure 26, presenting  $c_f$  as a function of the relative roughness. A dashed line is drawn through the data and labeled

$$1/\sqrt{c_f} = 4.06 \log_{10} \delta/k + 8.56 \quad (21)$$

In this equation the  $k$  of the screen was taken to be 0.009 foot.



Figures 28 and 29 indicate the variation of the shape parameter  $H$  as a function of the Reynolds number and the relative roughness, respectively. The variation of  $H$  with the Reynolds number in flow over smooth flat plates has been approximated by Tetervin and Lin [8] with the expression

$$\log_{10} H = 0.5990 - 0.1980 \log_{10} R_{\theta} + 0.0189 (\log_{10} R_{\theta})^2 \quad (22)$$

in which  $R = U\theta/\nu$ . A smooth curve representing the locus of points determined by the substitution in this equation data obtained in this investigation is drawn in Figure 28.

## DISCUSSION OF THE RESULTS

The Role of the Discharge

Discharge has an insignificant effect upon the thickness of the boundary layer at a fixed value of  $x$ . This fact is first evident in Figure 20, the plot of  $\delta$  as a function of  $x$ , and reappears in dimensionless form in Figures 24 and 25. One notes upon inspection of these plots that points corresponding to the same slope and the same boundary, but with much different rates of discharge, fall along the same line within the limits of experimental variation. This does not mean the same thickness at the same station; it is only with reference to the parameter  $x = U^2/2gS$  that the effect of variable discharge becomes indeterminable. This fact is basic to the solution of the full-scale problem. Evidently, one need only use the parameter  $x$  to define the location on the slope, and the development observed in the laboratory becomes identical to that occurring over the same boundary at any rate of discharge.

Of course, the discharge is significant in determining the depth of flow and hence the location of the critical point. In this sense it limits the growth of the boundary layer, so that knowledge of discharge is necessary to define that aspect of boundary-layer development. An illustrative example in the section "APPLICATION TO THE DESIGN PROBLEM" will demonstrate the role of the discharge in locating the critical point.

### The Role of the Slope

As in the case of the discharge, slope has little effect on the thickness of the boundary layer at a fixed value of  $x$ . Although a slight difference between the developments occurring over the different slopes is apparent in some instances, it will be shown in the illustrative example of the section "APPLICATION TO THE DESIGN PROBLEM" that no important difference in the calculated location of the critical point results from choosing first one and then the other of these slightly different values of  $\delta/x$ . As in the case of the discharge, knowledge of the slope is essential in the computation of the depth of flow and hence the location of the critical point. The illustrative example mentioned will also demonstrate the use of slope in this regard.

The effect of the slope upon  $c_f$  and upon  $H$  is similar to its effect upon  $\delta/x$ , with consistent variation being apparent only in some instances. In the case of the rough boundary, both  $\delta/x$  and  $c_f$  seem to have a positive correlation with slope. A more indistinct trend in the same direction is indicated in the plot for  $H$  as a function of relative roughness. The effect in the case of the smooth boundary is indeterminable, however.

### The Role of the Boundary Roughness

Of all the variables employed in the investigation, the roughness of the boundary proved to be the most significant in determining the locus of the nominal thickness of the turbulent boundary layer. One notes first of all in Figure 20 that all of the points

follow two distinct trends, one for the smooth boundary and one for the rough. Again in Figures 24 and 26, this grouping according to roughness is evident, although the nature of Figure 24 is such that the delineation is not as distinct as it is in Figure 20.

The difference between the two trends evident in Figure 24 is greatest in the middle range of Reynolds numbers, being small at very low and at very high Reynolds numbers. This is to be expected, in view of the fact that at very low Reynolds numbers the flow within the boundary layer is laminar so that roughness of the boundary is of no consequence, and also in view of the fact that as  $R = Ux/\nu$  increases with  $x$  the thickness of the boundary layer is so large compared to the height of the roughness  $k$  that the boundary again becomes effectively smooth. This latter fact is very significant to the spillway problem, for it makes possible at high Reynolds numbers a useful calculation of the location of the critical point without a precise specification for the roughness of the boundary.

It should be repeated at this point that the roughness of the screen used in the laboratory investigation is probably greater than that encountered on most concrete spillways. The variation of the parameter  $\delta/x$  on an actual concrete spillway, then, should lie somewhere between that associated with the glass boundary and that associated with the screen boundary. Even if the concrete were as rough as the screen, however, the effect on the location of the critical point would not be great. It may be surmised on this basis that,

with the possible exception of the crest region, a very smooth spillway surface is not economically justified.

Summarizing the discussion up to this point, slope and discharge are unimportant as far as the rate of growth of the boundary layer is concerned. The roughness of the boundary is significant near the crest, becoming less important with increasing distance along the slope.

### The Nominal Thickness of the Boundary Layer

We turn next to a consideration of the nature of the variation of the boundary-layer thickness. At high Reynolds numbers on both smooth and rough boundaries,  $\delta$  is nearly a linear function of  $x$ . This is especially true with the smooth boundary. It is true that the ratio of  $\delta/x$  continues to decrease as the Reynolds number increases; its rate of change is small enough, however, that very little curvature of the locus  $y = \delta$  results. Solution of the problem given in the illustrative example will demonstrate this fact.

Turning for a moment to  $\theta$ , one gains an insight into the nature of its variation in the light of the von Karman momentum equation solved for  $d\theta/dx$ :

$$\frac{d\theta}{dx} = \frac{1}{2} (c_f - (H+2) \frac{\theta}{x}) \quad (23)$$

We see here that the gradient of  $\theta$  with respect to  $x$  is a function of the difference between two terms, both of which are decreasing in magnitude in the  $x$  direction. In the usual case,  $c_f$  decreases more

rapidly than does  $\theta/x$ , so that the locus of  $\theta$  is slightly concave downward. The nature of the equation is such, however, that little curvature is possible.

Going back to  $\delta$ , a significant effect is evident in the relationship between  $H$ ,  $\delta$ , and  $\theta$ . Making the assumption that the velocity profile may be characterized by an expression of the form  $u = m y^n$ , applying the definition of  $\theta$ , and solving for the ratio of  $\delta/\theta$  in terms of  $H$ , we have:

$$\frac{\delta}{\theta} = \frac{H(H+1)}{H-1} \quad (24)$$

The significance of this expression lies in the fact that  $H$  is approaching unity in the region of interest. The denominator of the fraction on the right side of the equation therefore decreases more rapidly than does the numerator. This means that  $\delta$  is an increasing multiple of  $\theta$ , as it is as the shape of the velocity profile progresses in the direction of a rectangular distribution. Thus it is necessary that the locus of  $\delta$  with respect to  $x$  be less concave in the direction toward the boundary than is the locus of  $\theta$  with respect to  $x$ . It is entirely possible, therefore, that the locus of  $\delta$  with respect to  $x$  is actually linear at high Reynolds numbers, even if the locus of  $\theta$  is not.

In the case of the rough boundary, the pronounced curvature of the locus of  $\delta$  with respect to  $x$  is due primarily to the

continuing decrease in the relative roughness, producing a more rapid change in the value of  $c_f$  as a function of  $x$  than is observed in the case of the smooth boundary. As the relative roughness approaches the limit at which it is effectively smooth, however, the variation in  $c_f$  will decrease and at the same time the value of  $H$  will be near unity so that again the locus of  $\delta$  with respect to  $x$  is possibly linear.

#### The Shape of the Velocity Profile

The shape of the velocity profile associated with the development of the turbulent boundary layer on steep slopes is better approximated in most regions by an expression of the form  $u = m y^n$  than one of the form  $u = b \log y$ . This is especially true at large Reynolds numbers; it is not true at low Reynolds numbers and within close proximity of the boundary. Examination of Figures 10 through 17 with the aid of a straight edge will reveal this fact. On the other hand, the expression of Tetervin and Lin, Equation (22), obtained from consideration of boundary-layer developments over flat plates with zero pressure gradient, is an approximation to the values of  $H$  obtained experimentally. Figure 28 indicates the degree of agreement. Evidently, the effect of continuous acceleration over the experimental range has little bearing on the value of  $H$  expressed as a function of  $U\theta/\nu$ , as it is in Equation (22). In the opinion of the author the value of  $H$  in boundary-layer development on steep slopes does not subsequently increase, however, according to the predictions of

Equation (22) but continues to decrease although at a diminishing rate. This is based upon the consideration that large values of  $H$  are associated with imminent separation. It is impossible to imagine imminent separation in flow down steep slopes.

#### The Coefficient of Boundary Shear for the Glass

Application of the Karman-Prandtl velocity-distribution equation for turbulent flow near smooth boundaries, Equation (4), to the turbulent boundary layer on the glass steep slope yields an expression for  $c_f$  which is an excellent approximation to the results obtained experimentally. This is evident upon examination of the relative position of the smooth curve and the points plotted for the glass boundary in Figure 26. Halbronn (10) made essentially this assumption in his method of synthesis of the development. Evidently, the presence of acceleration has little influence upon the ratio between the intensity of boundary shear and the dynamic pressure at the edge of the boundary layer. In other words, despite the fact that the shape of the velocity profile within the boundary layer is different from that associated with flow in a pipe, the intensity of boundary shear is the same for the same maximum velocity, the same density, and the same Reynolds number.

#### The Coefficient of Boundary Shear for the Screen

In like manner, application of the Karman-Prandtl velocity-distribution equation for turbulent flow near rough boundaries, Equation (5),



to the turbulent boundary layer on the steep slope with the screen boundary, yields an expression for  $c_f$  which is in excellent agreement with the experimental results if one chooses the value of  $k$  for the screen to be a great deal less than the value indicated by a test of the screen in uniform flow in an open channel. The value of  $k$  which gives an expression equivalent to one derivable from Equation 5 is 0.0021 feet; the value indicated by the test in uniform flow was 0.009 feet. The value of 0.0021 feet is very nearly the thickness of the screen, two wire diameters being 0.017 feet. One will note, however, that both values of  $k$  indicate a roughness comparable to concrete; corresponding values of  $n$  are 0.012 and 0.015.

Any derivation of  $c_f$  as a function of relative roughness which assumes the boundary shear to be composed entirely of form drag on elements of roughness, and which approximates the velocity profile by an expression of the form  $u = b \log y$ , will yield an expression of the form

$$1/\sqrt{c_f} = A \log \delta/k + B \quad (25)$$

in which the ratio between  $A$  and  $B$  is the logarithm of 30, 1.477. If, however, one makes the assumption that the distribution of the velocity is of the form  $u = m y^n$ , one arrives at an expression of somewhat different form. Doing this and deliberately arranging it

to resemble Equation (25), we have

$$\text{Log } 1/\sqrt{C_f} = n \text{ Log } \delta/k + C \quad (26)$$

in which  $n$  is the exponent in the expression  $u = m y^n$ ,  
and  $C$  is a constant which depends upon the shape of the  
velocity profile, and the height, shape, and density of the roughness.

In the opinion of the author, the actual value of the roughness of the screen as expressed by a magnitude for  $k$  remains in doubt over a range of values all of which are associated with various concrete surface textures. The fact that it lies within this range, however, is sufficient to render the observations made in flow over the screen very useful, as will be demonstrated in the following illustrative example.

## APPLICATION TO THE DESIGN PROBLEM

Outline of the Method of Approach

The design problem contemplated herein requires the location of the critical point for a given discharge on a given spillway and the calculation of the water-surface profile upstream from that point. The location of the critical point is determined by the graphical intersection of the projection of the locus of the nominal thickness of the turbulent boundary layer with the projection of the locus of the free surface. The locus of the nominal thickness of the boundary layer is determined with reference to either Figure 24 or 25, depending upon the roughness of the surface. The locus of the free surface is determined by adding to the depth of the potential flow the displacement thickness of the boundary layer, which is assumed to be from  $1/8$  to  $1/10$  of the thickness of the boundary layer, depending upon the magnitude of the Reynolds number.

Illustrative Example

Consider a concrete spillway of indefinite length with a slope of 0.80 and a roughness such that  $k$  is 0.005 feet. Let it be required to locate the critical point and the line of the free surface when the discharge is 360 cubic feet per second per foot of spillway width.

We shall make use of the line labeled "Design Curve" on Figure 25, performing the computations in tabular form as follows:

$x$	$x/k$	$\delta/x$	$\delta$	$U^2/2g$	$q/U$	$y_0$
50	$1 \times 10^4$	0.0073	0.36	40	7.09	7.13
100	$2 \times 10^4$	0.0066	0.66	80	5.00	5.07
200	$4 \times 10^4$	0.0060	1.20	160	3.53	3.65
400	$8 \times 10^4$	0.0055	2.20	320	2.50	2.72
600	$1.2 \times 10^5$	0.0052	3.12	480	2.04	2.35

The column headed  $x$  is taken to be any reasonable value of distance along the slope at which the location of the water surface is desired. The value of  $x/k$  is the value of  $x$  divided by 0.005 feet. The value of  $\delta/x$  is read from the design curve on Figure 25. The value of  $\delta$  is obtained by multiplication of the first and third columns. The value of  $U^2/2g$  is by definition the product of the slope and  $x$ , in this case  $0.80x$ . Having determined the value of  $U$  from the known magnitude of the velocity head, we divide the discharge per foot by it to obtain the potential thickness of flow,  $q/U$ . To this we add 10% of the thickness of the boundary layer to determine the actual thickness of the flow, listed as  $y_0$  in the last column.

The best method of locating the critical point involves plotting the values of  $\delta$  and  $y_0$  obtained in the preceding table as functions of  $x$ . It is convenient to use log-log paper for this purpose because of the great difference between the depth of flow and the thickness of the boundary layer in the upper portions of the flow.

This is illustrated in Figure 30, in which both the locus of the nominal thickness of the boundary layer and that of the free surface are shown.

In order to illustrate the effect of change in the roughness, the calculation process was repeated using the same situation but with a roughness twice as large, i.e., 0.01 feet. The line labeled " $y = \delta$ ,  $k = 0.01'$ " is the result of this computation. One will note that the difference between the values of  $x$  for the two cases is about 30 feet in 450 feet, or a variation of less than 10%.

One will note that the order of magnitude of the changes in  $\delta/x$  produced by a difference in slope is less than that involved in changing the roughness twofold. Thus the single design curve on Figure 25 will suffice for all slopes.

Once the value of  $x$  at the critical point has been determined, the corresponding station on the slope may be located by measuring the value of  $x$  in feet along the slope. The origin of coordinates is the intersection with the line of total head of a line drawn parallel to the slope through the water surface at the critical point. This procedure merely satisfies the definition of  $x$ .

## CONCLUSIONS

1. Aside from their respective influences upon the location of the free surface and the magnitude of the potential velocity, neither the slope of the boundary nor the magnitude of the discharge is significant in determining  $\delta$  as a function of  $R = Ux/\nu$  or as a function of  $x/k$ , while the magnitude of the boundary roughness is the most significant variable in this respect, its influence decreasing with increase in the boundary-layer thickness.
2. Applications of the Kármán-Prandtl velocity-distribution equations for turbulent flow near smooth and near rough boundaries to the turbulent boundary layer as it develops on both smooth and rough steep slopes yield expressions for  $c_f$  which are excellent approximations to the results obtained experimentally. In the case of the rough boundary, however, such agreement requires the use of a value of  $k$  considerably less than that determined by testing the same roughness in uniform flow in an open channel.
3. The shape of the velocity profile within the turbulent boundary layer as it develops on smooth steep slopes is little different from that observed in flow past flat plates, while that associated with the rough boundary is considerably less block-like at the same Reynolds number. In both instances, an expression of the form  $u = m y^n$  is a better characterization of the velocity distribution than one of the form  $u = b \log y$ .

4. At large distances along a steep slope the quantity  $d\delta/dx$  is nearly constant and not greatly different for the various roughnesses encountered on concrete spillways. For this reason, a useful calculation of the location of the critical point may be made without a precise specification for the value of  $k$  .

## REFERENCES

- [1] Prandtl, L., "Über Flüssigkeiten bei sehr kleiner Reibung," Verhandlung III Intern. Math. Kongress, Heidelberg, 1904.
- [2] von Kármán, Th., "Laminare und turbulente Reibung," Zeitschrift für angewandte Mathematik und Mechanik, Bd. 1, p. 235, 1921.
- [3] Rouse, Hunter, "Elementary Mechanics of Fluids," John Wiley & Sons, Inc., 1946.
- [4] Nikuradse, J., "Strömungsgesetze in rauhen Rohren," VDI-Forschungsheft 361, Berlin, 1933.
- [5] Schlichting, H., "Boundary Layer Theory", NACA TM 1217 and 1218, Washington, 1949.
- [6] Gruschwitz, E., "Die turbulente Reibungsschicht in ebener Strömung bei Druckabfall und Druckanstieg," Ing.-Arch., Bd. II, p. 321, 1931.
- [7] von Doenhoff, A.E., and Tetervin, N., "Determination of General Relations for the Behavior of Turbulent Boundary Layers," NACA Report 772, 1943.
- [8] Tetervin, N., and Lin, C.C., "A General Integral Form of the Boundary-Layer Equation for Incompressible Flow with an Application to the Calculation of the Separation Point of Turbulent Boundary Layers," NACA TN 2158, August 1950.
- [9] Granville, P.S., "A Method for the Calculation of the Turbulent Boundary Layer in a Pressure Gradient," the David W. Taylor Model Basin, Navy Department Report 752, May 1951.
- [10] Halbronn, G., "Étude de la mise en régime des écoulements sur les ouvrages a forte pente," Thesis, Université de Grenoble, 1951.
- [11] Hickox, G.H., "Air Entrainment on Spillway Faces," Civil Engineering, Vol. 15, No. 12, p. 562, December 1945.



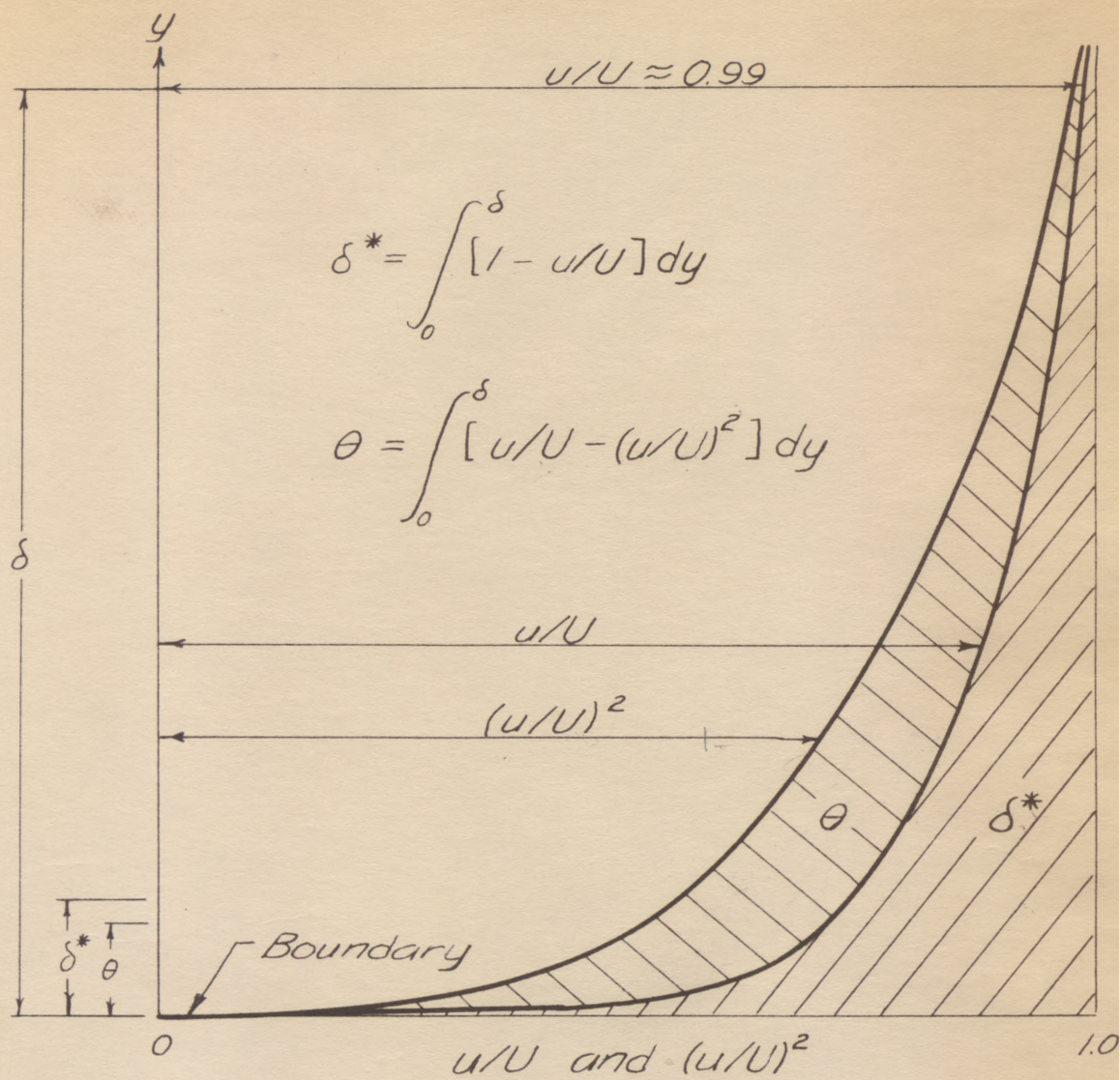


Figure 1. Definitions of  $\delta$ ,  $\delta^*$ , and  $\theta$ .

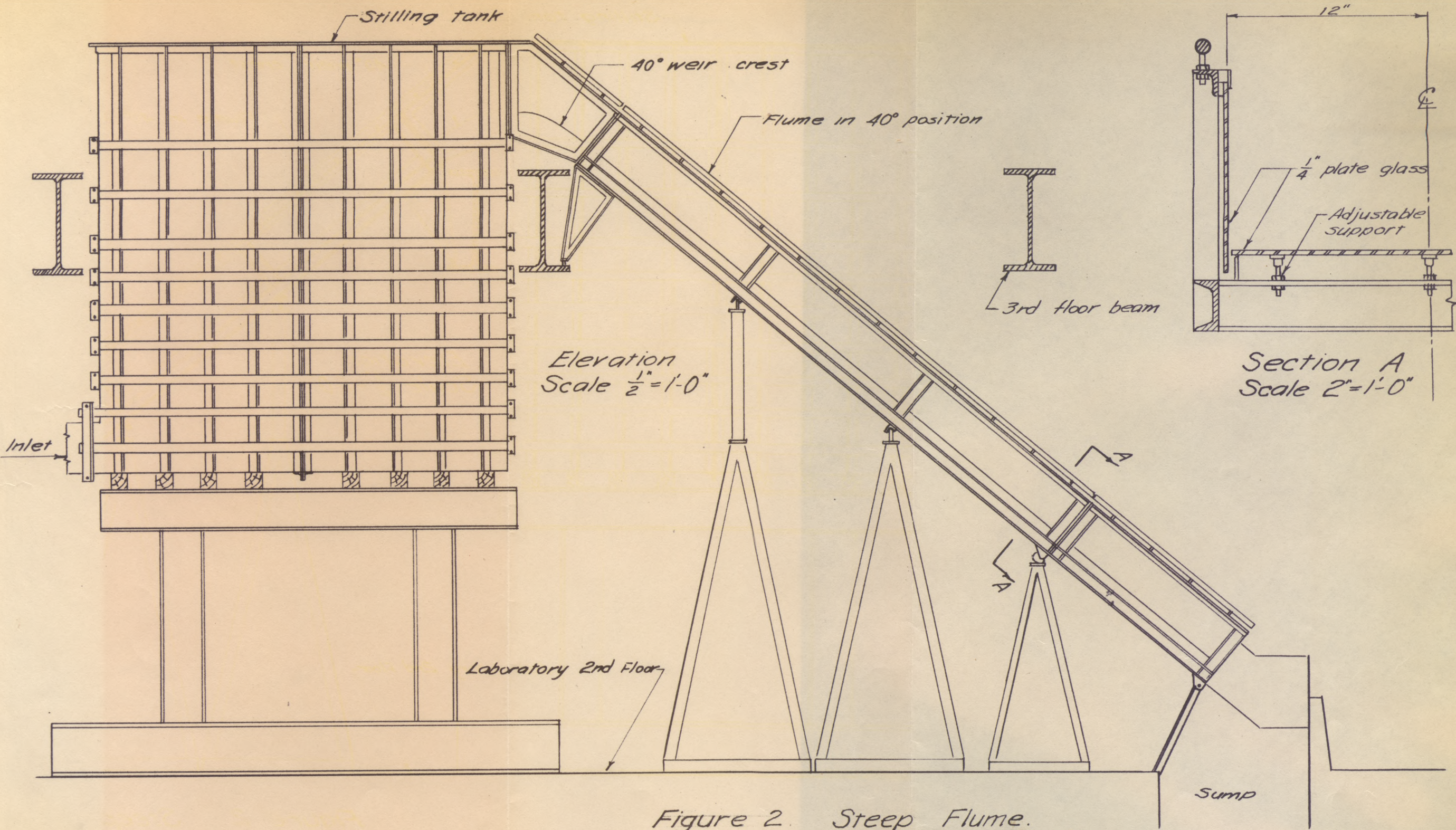


Figure 2 Steep Flume.

(a)  $20^\circ$  Slope



(b)  $40^\circ$  Slope

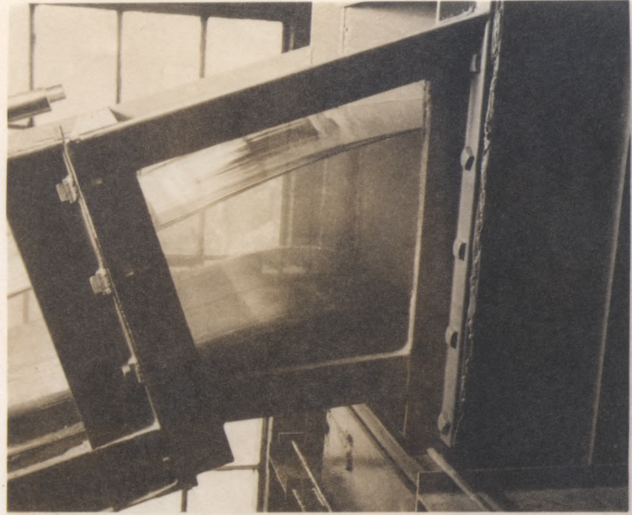


(c)  $60^\circ$  Slope

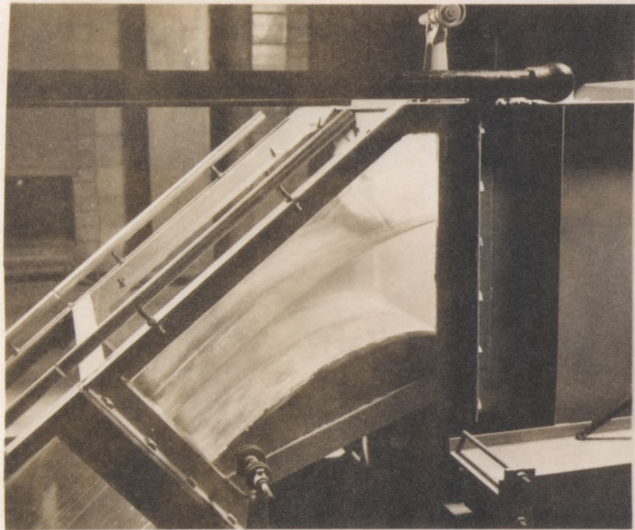


Figure 3. General Views of Flume.

(a)  $20^\circ$  Slope



(b)  $40^\circ$  Slope



(c)  $60^\circ$  Slope

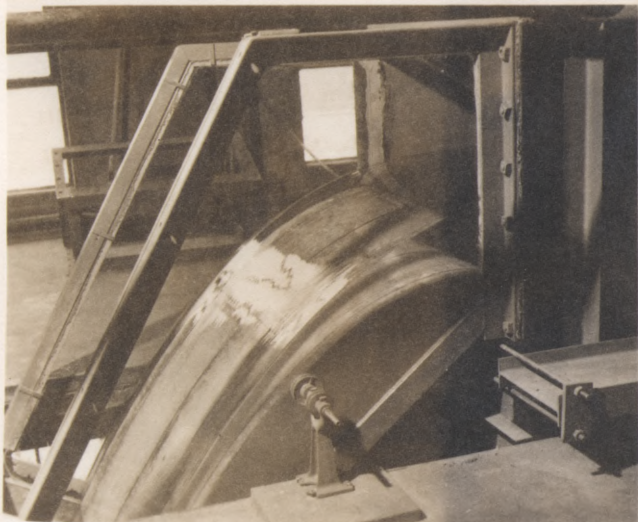
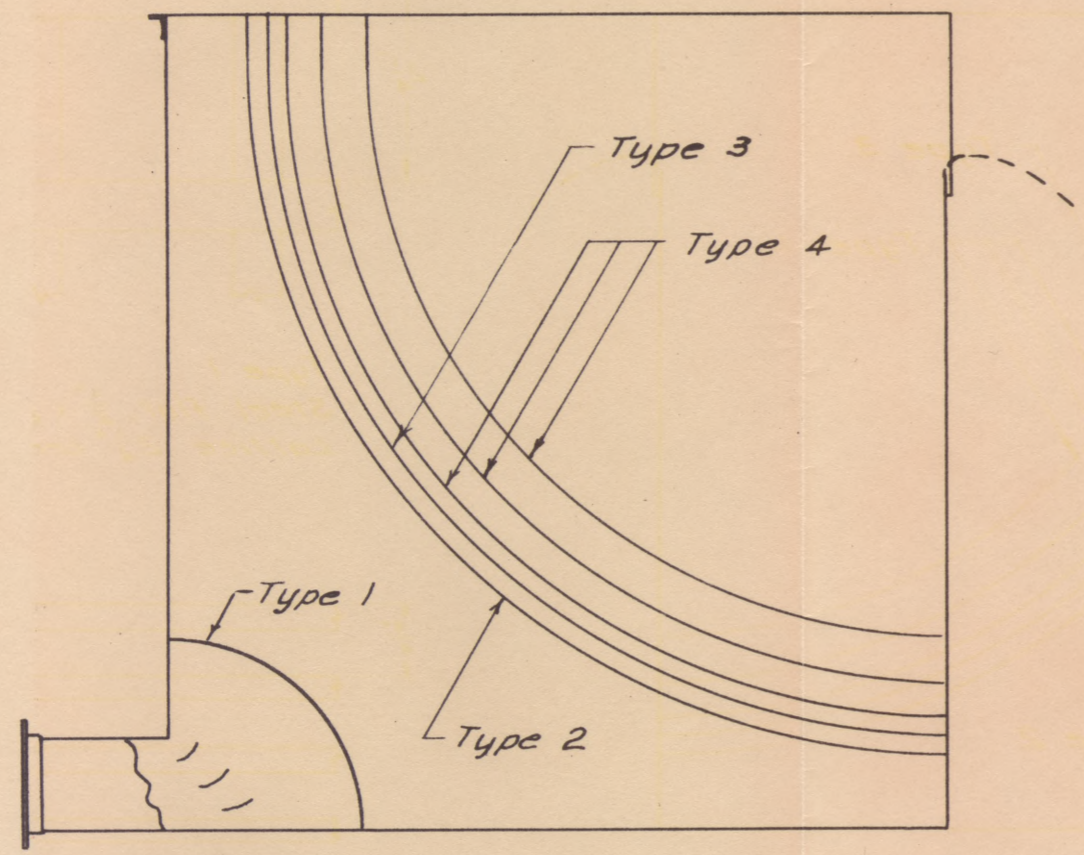
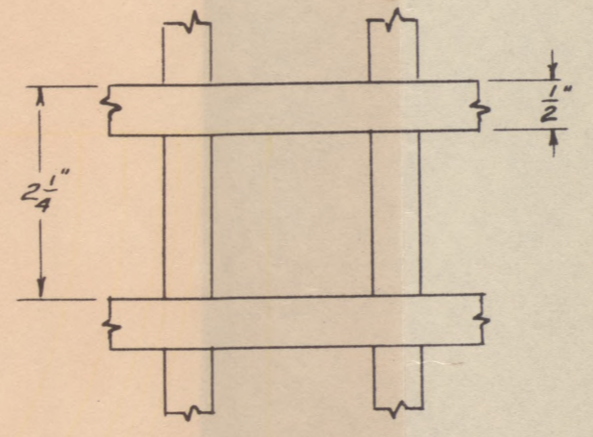


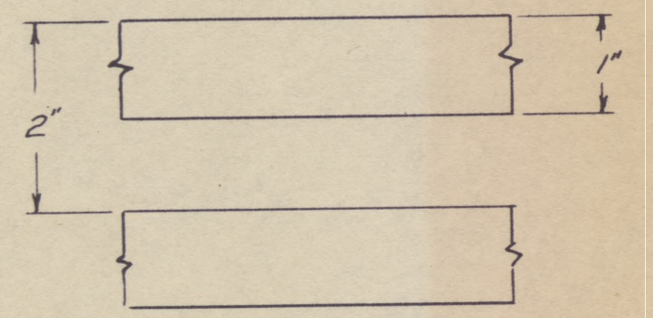
Figure 4. General Views of Crests.



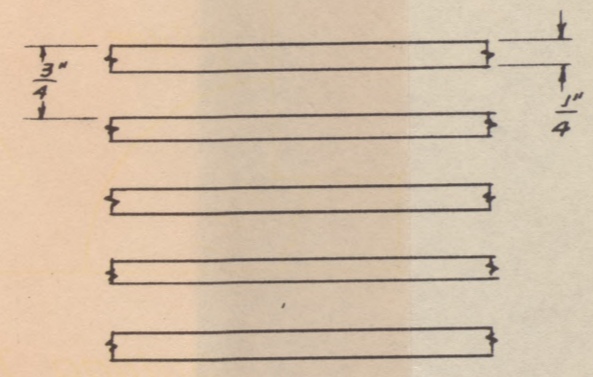
Stilling Tank, Sectional View  
Scale  $\frac{1}{2}'' = 1'-0''$



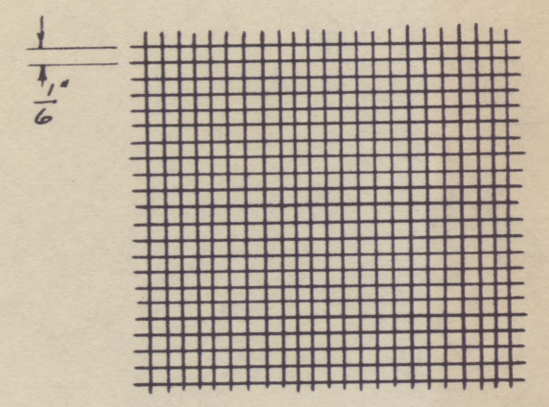
Type 1  
Steel flat,  $\frac{1}{2}'' \times \frac{1}{8}''$   
Lattice  $2\frac{1}{4}''$  centers.



Type 2  
Wood strips,  $1'' \times 1''$   
Grid  $2''$  centers.



Type 3  
Wood strips,  $\frac{1}{4}'' \times 1''$   
Grid  $\frac{3}{4}''$  centers.

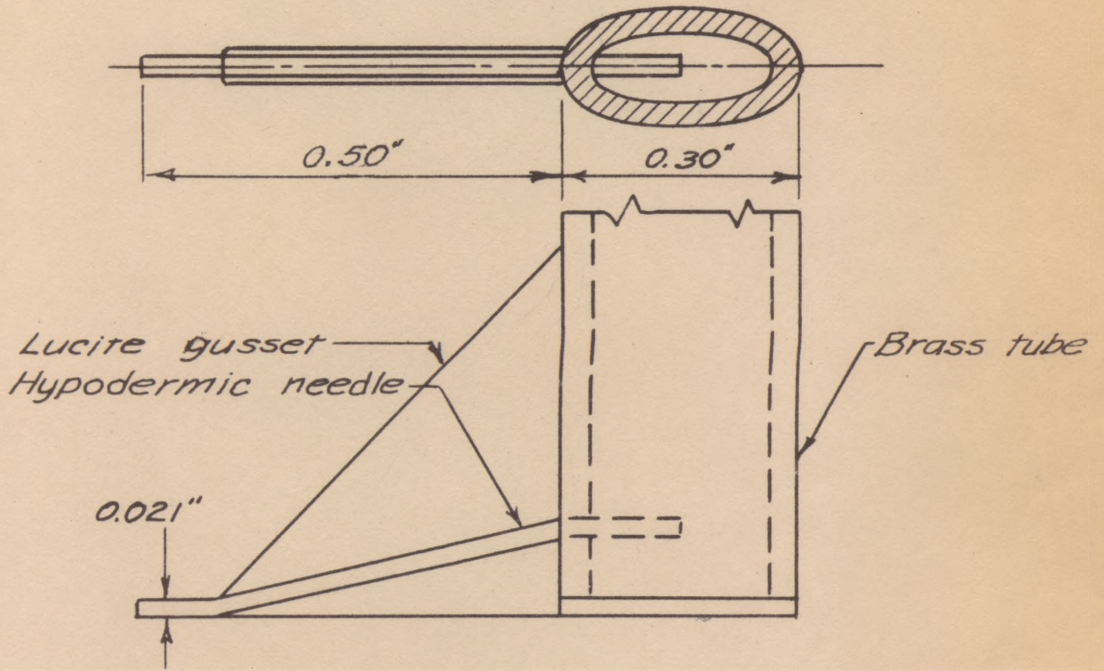


Type 4  
Steel wire,  $0.032''$  dia.  
Mesh 6 wires/inch.

Figure 5. Stilling Tank Details.

Scale 1" =  $\frac{1}{4}$ "

(a) Smaller stagnation tube.



(b) Larger stagnation tube.

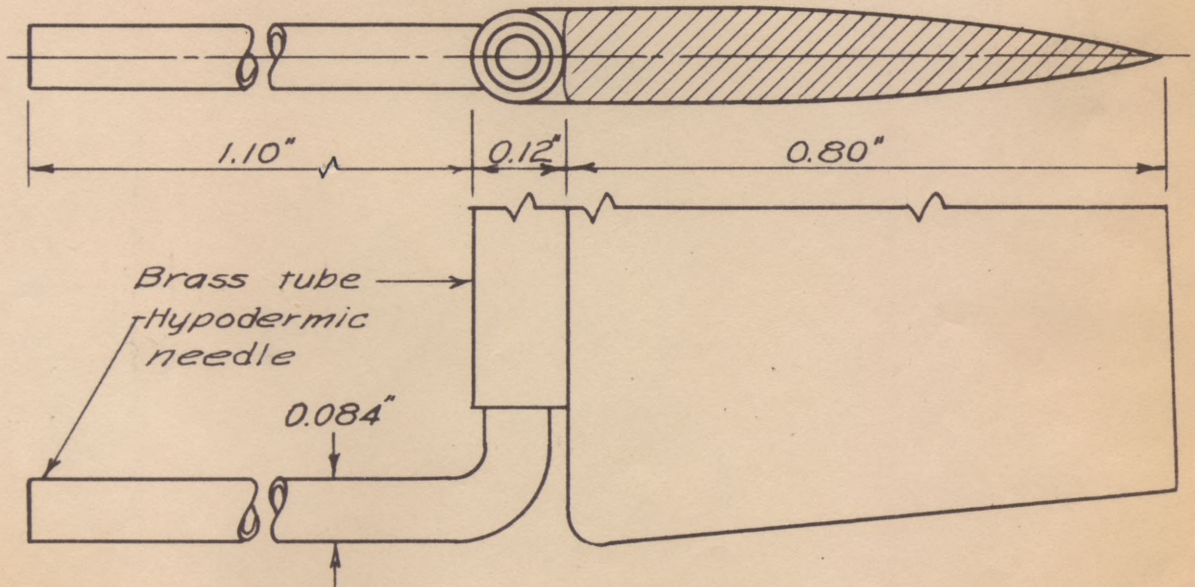


Figure 6. Stagnation Tubes.

Figure 7  
 Scale 1"=1'-0"  
 Maximum discharge on 20° slope

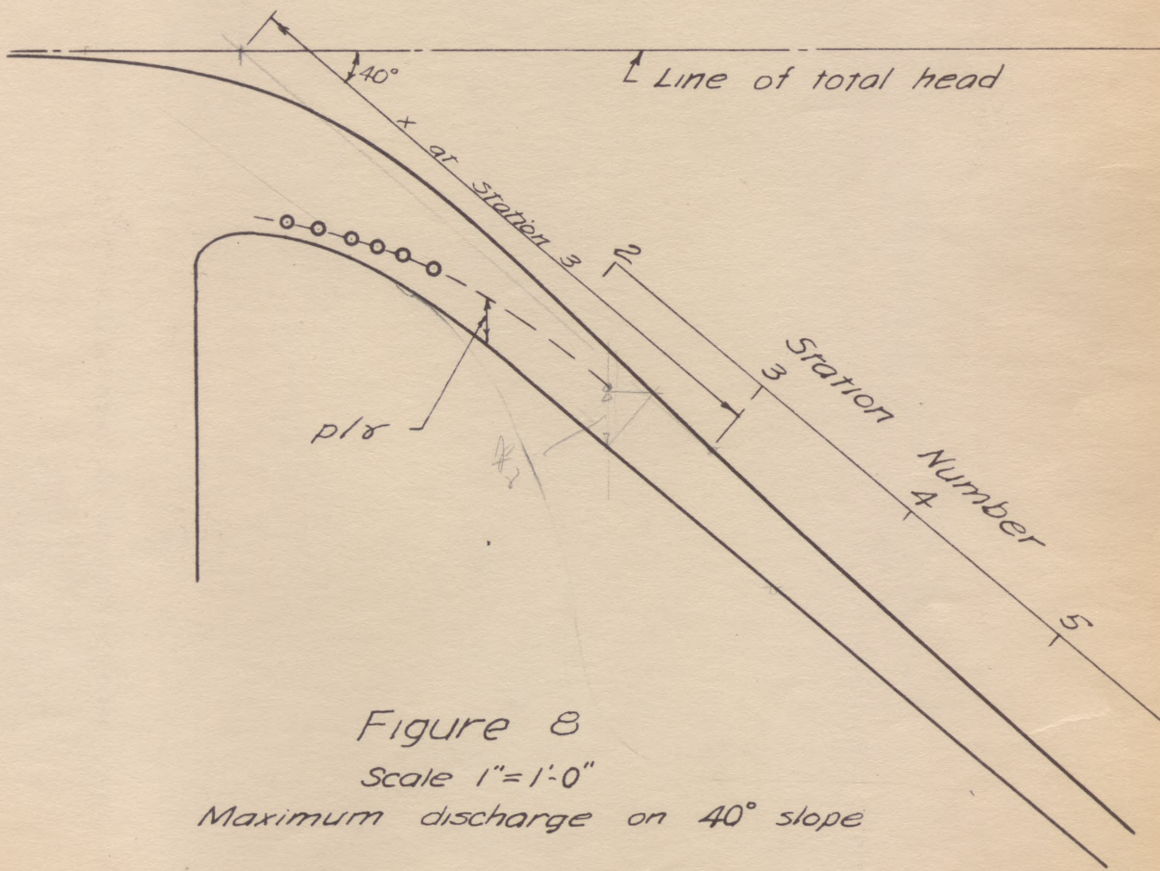
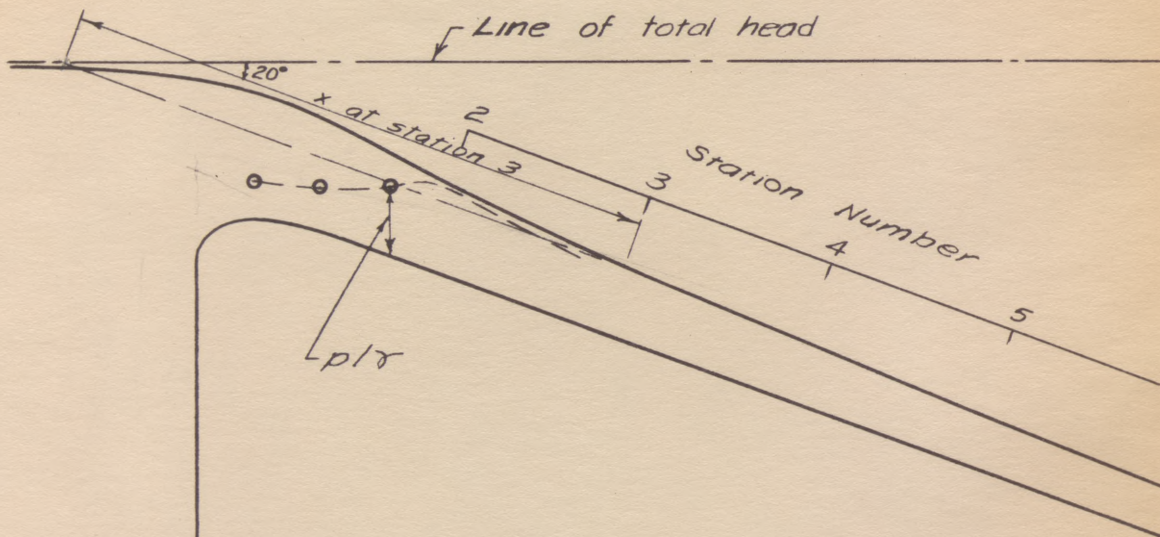


Figure 8  
 Scale 1"=1'-0"  
 Maximum discharge on 40° slope

Scale 1" = 1'-0"  
 Maximum discharge on 60° slope

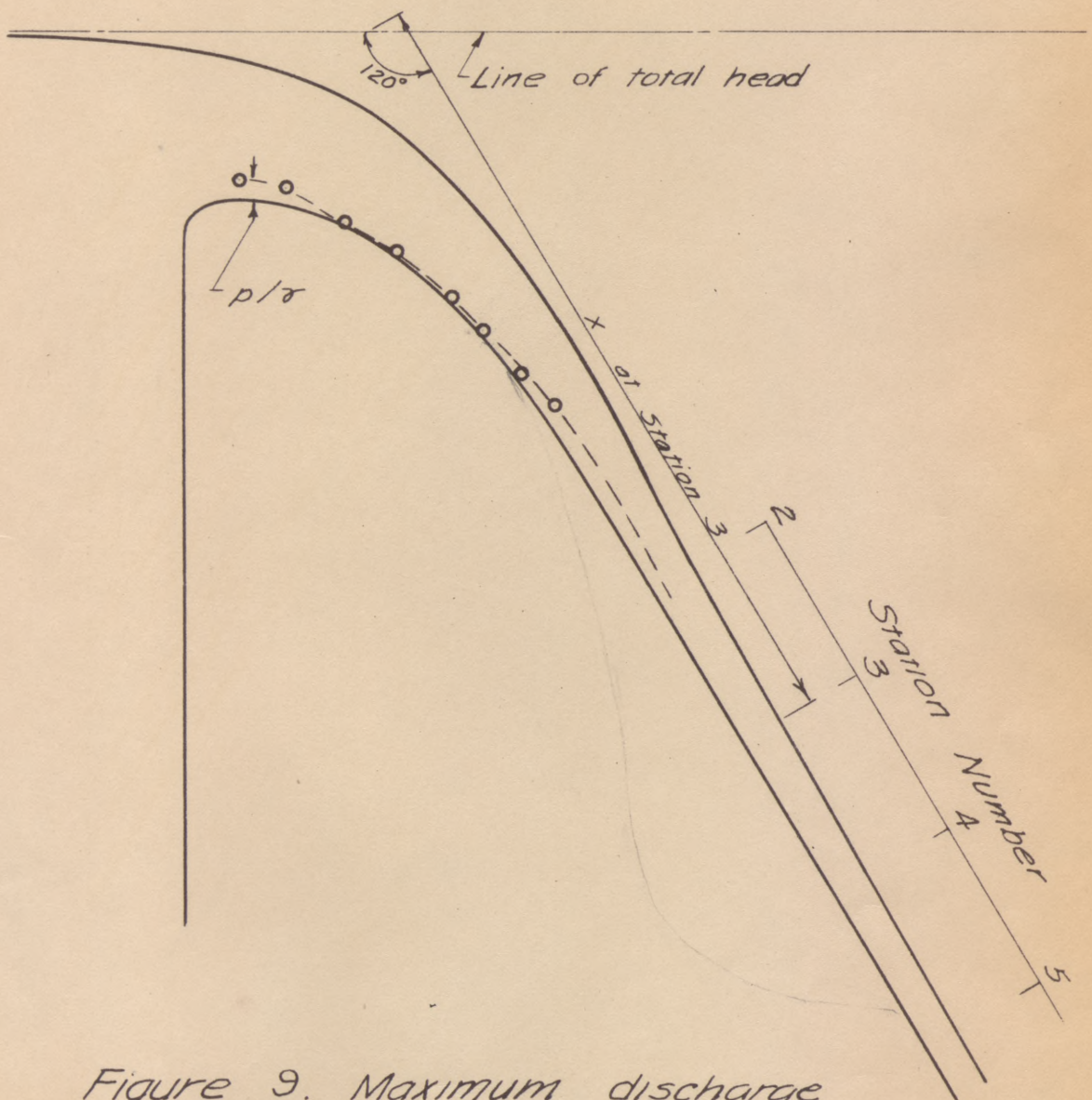


Figure 9. Maximum discharge on 60° slope.



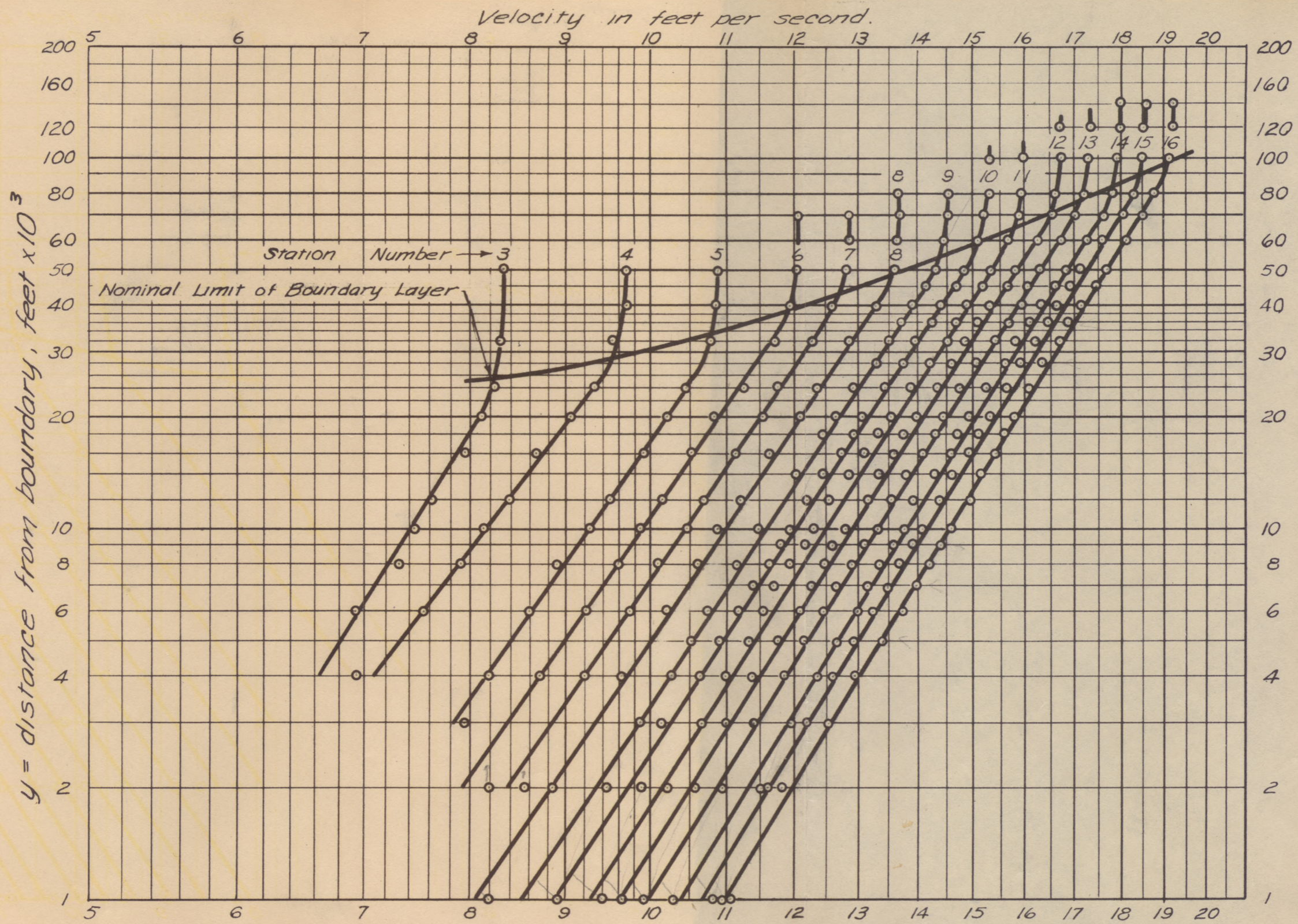


Figure 10. Velocity Profiles, Glass Boundary, 20° Slope, 2.98 cfs/ft

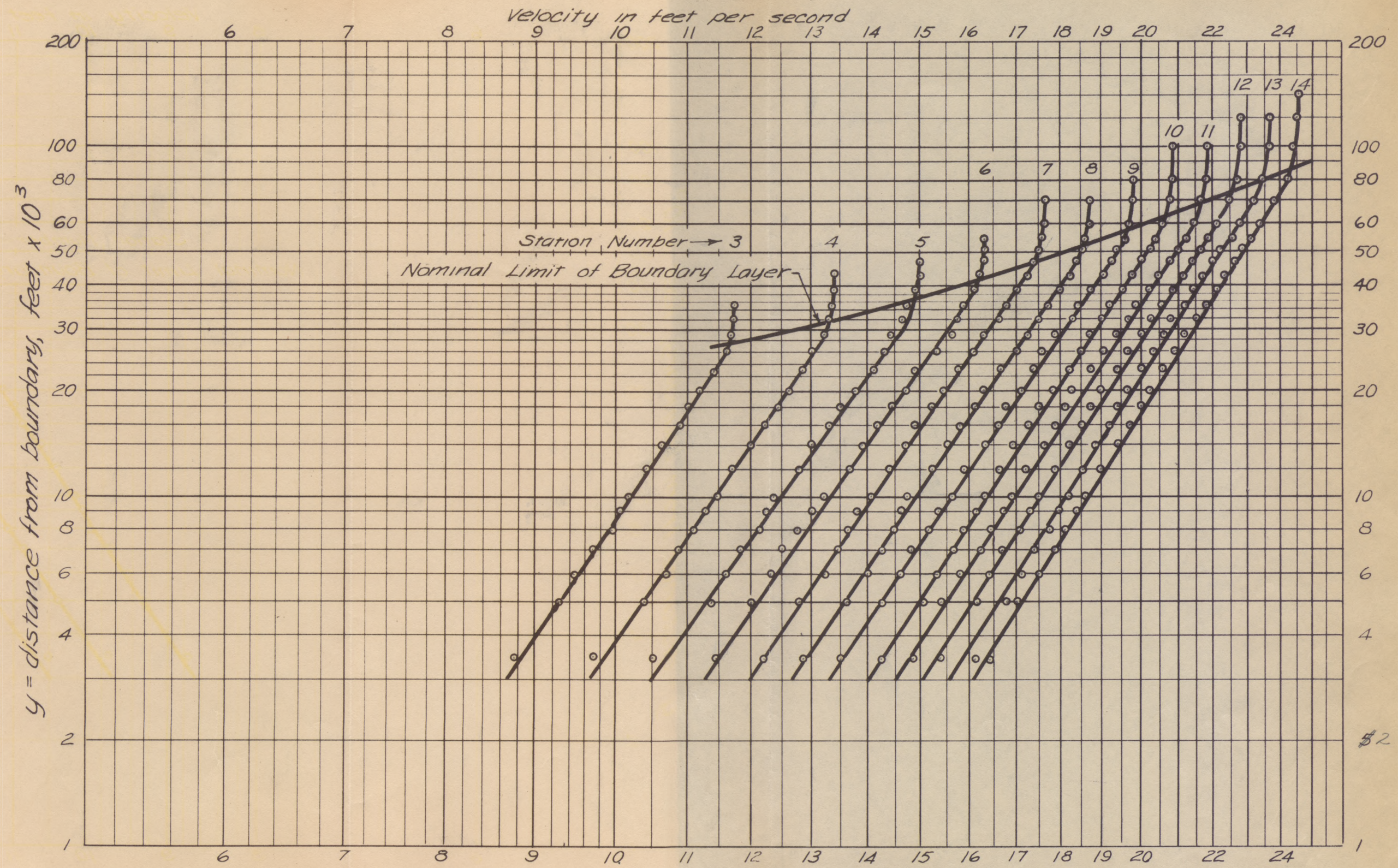


Figure 11. Velocity Profiles, Glass Boundary, 40° Slope, 3.68 cfs/ft

52

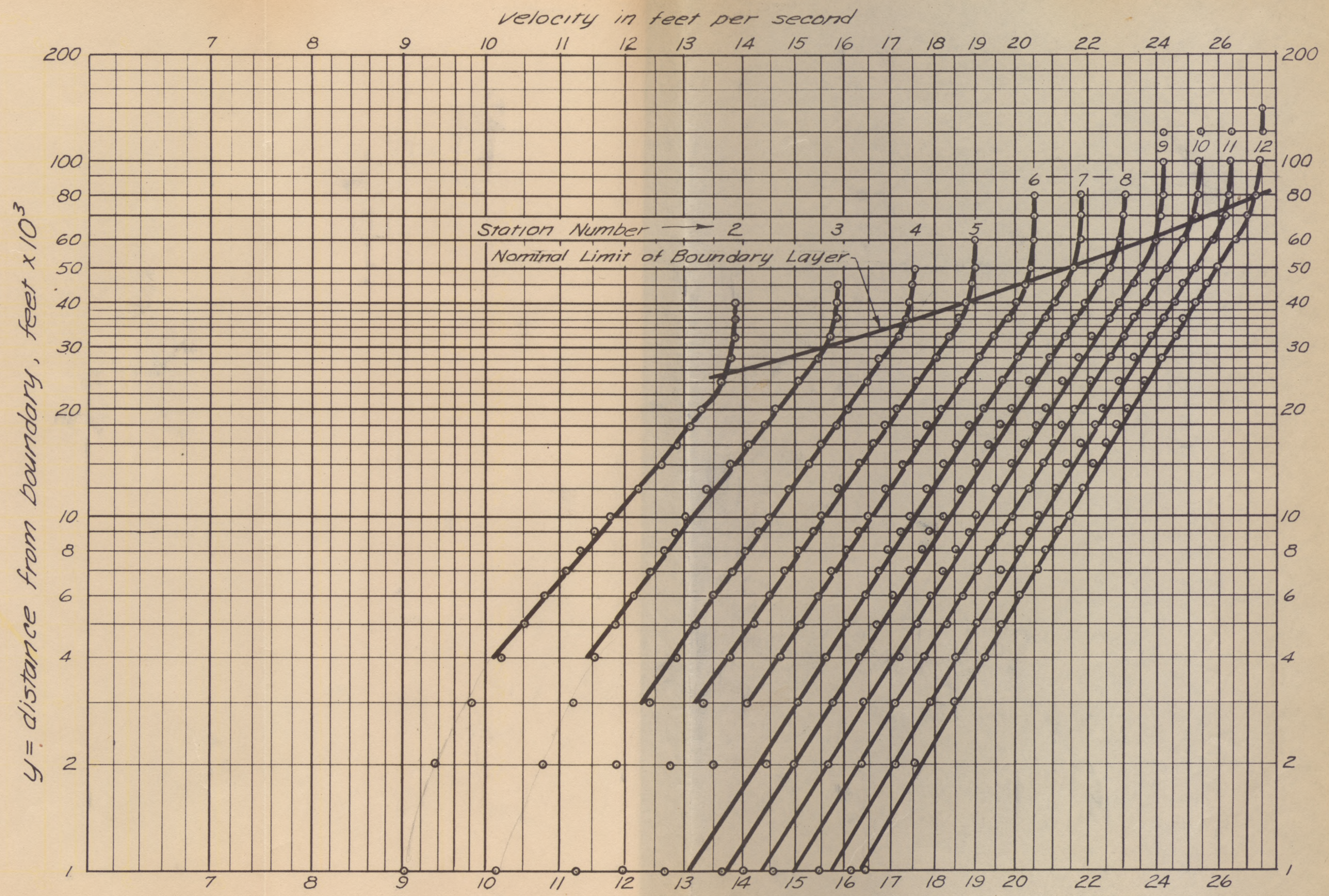


Figure 12. Velocity Profiles, Glass Boundary, 60° Slope, 3.65 cfs/ft.

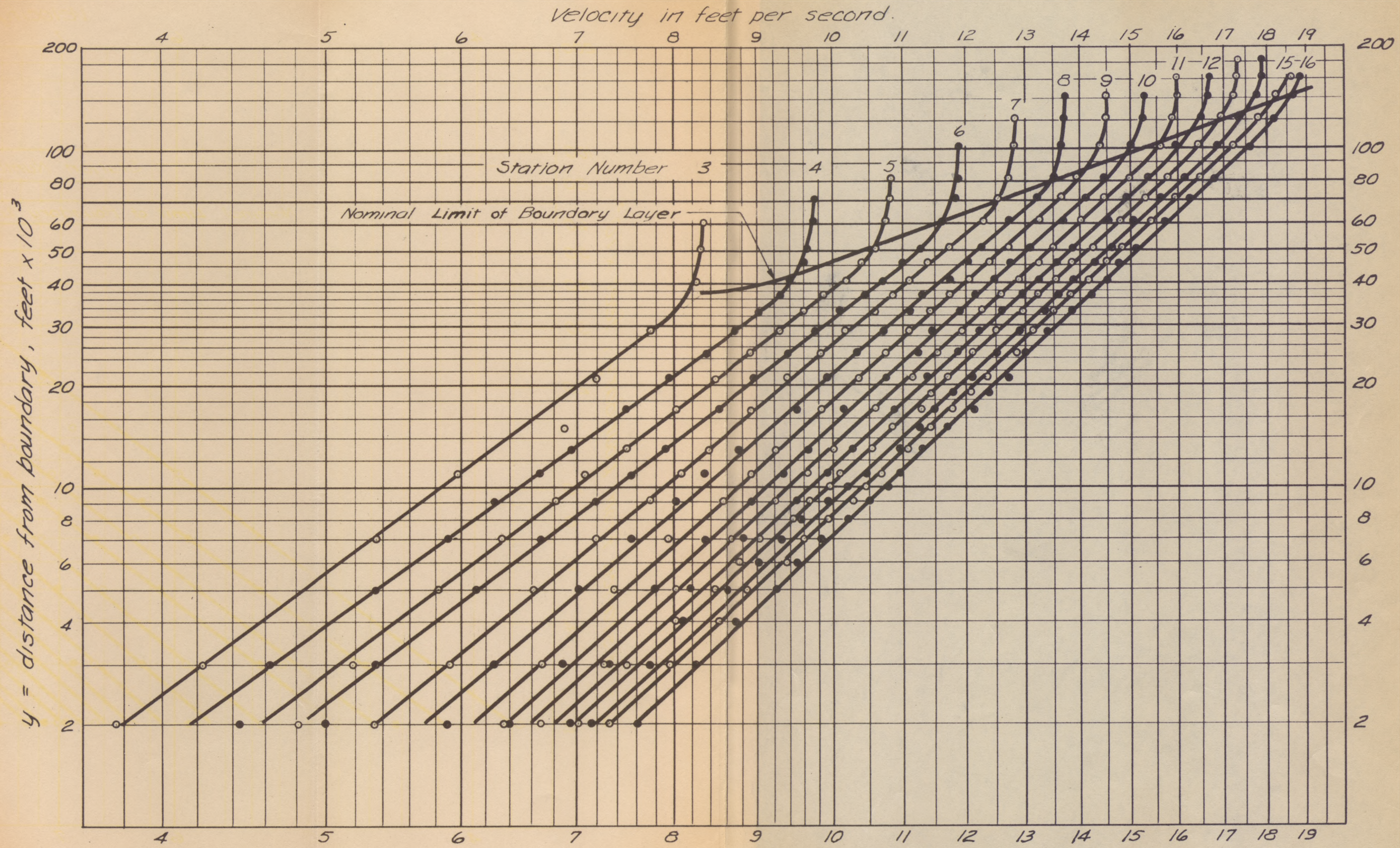


Figure 13. Velocity Profiles, Screen Boundary, 20° Slope, 2.98 cfs/ft

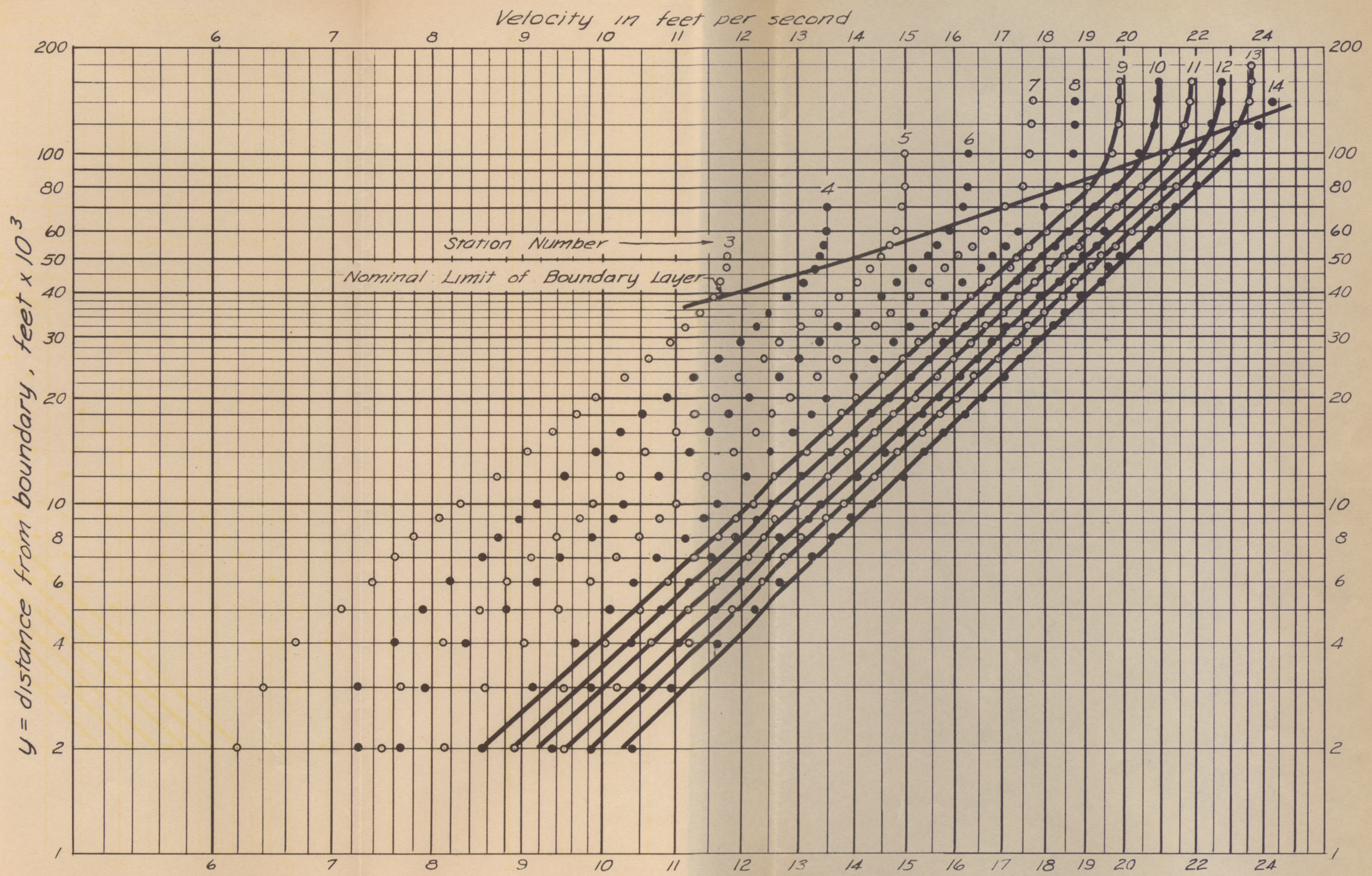


Figure 14. Velocity Profiles, Screen Boundary, 40° Slope, 3.68 cfs/ft

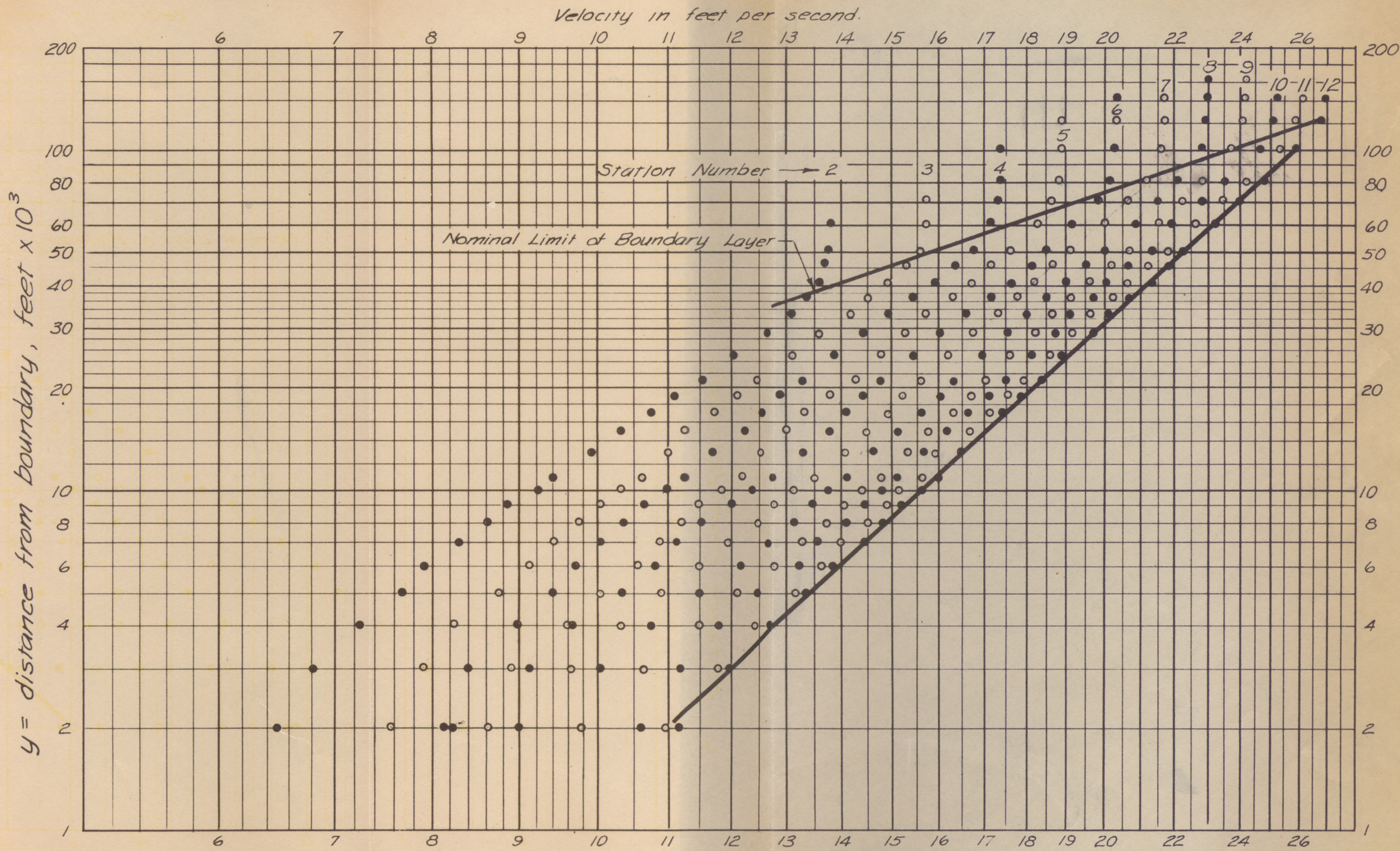


Figure 15. Velocity profiles, Screen Boundary, 60° Slope, 3.65 cfs/ft

Velocity in feet/second

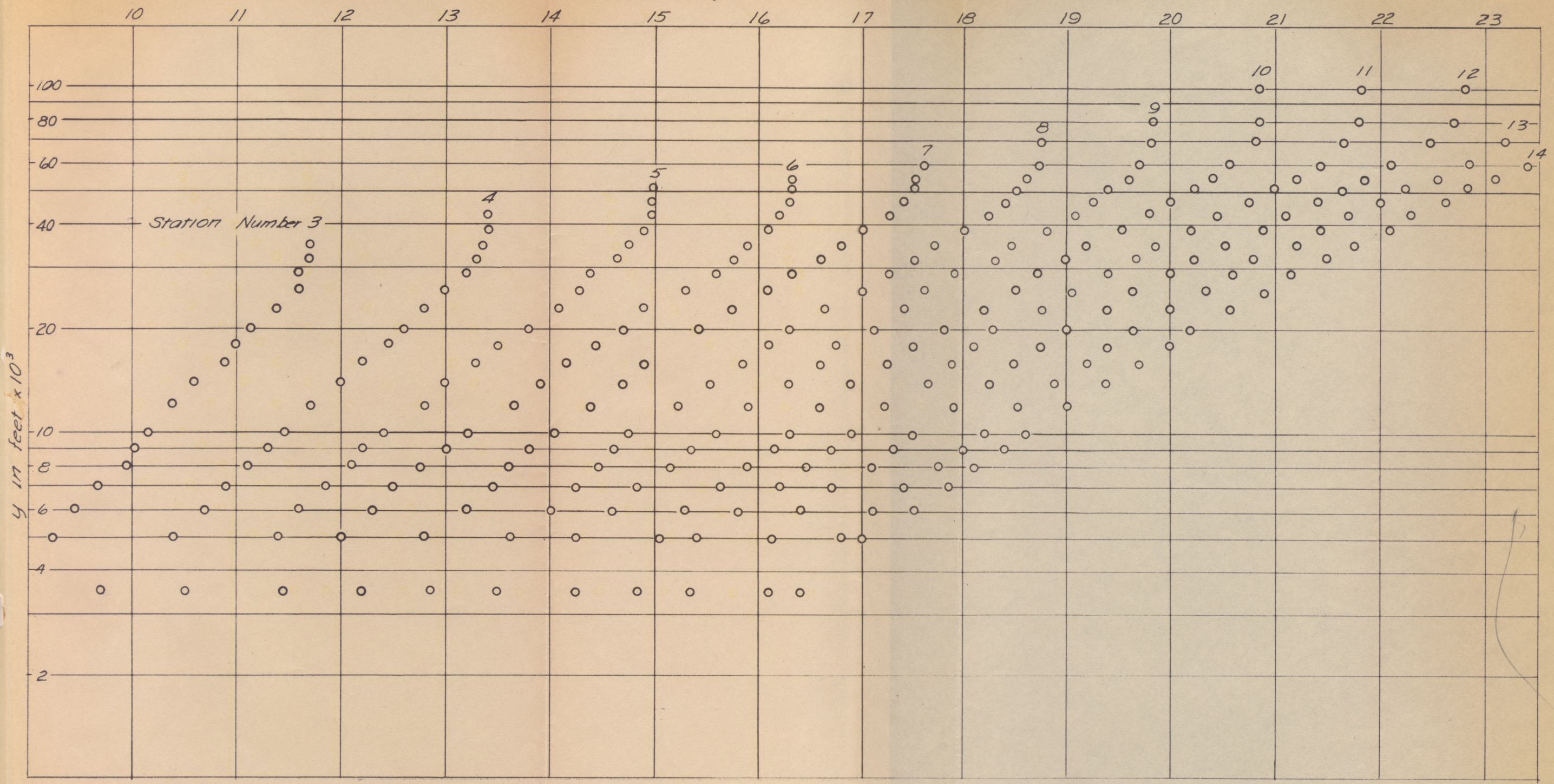


Figure 16. Velocity Profiles, Glass Boundary, 40° Slope, 3.68 cfs/ft.

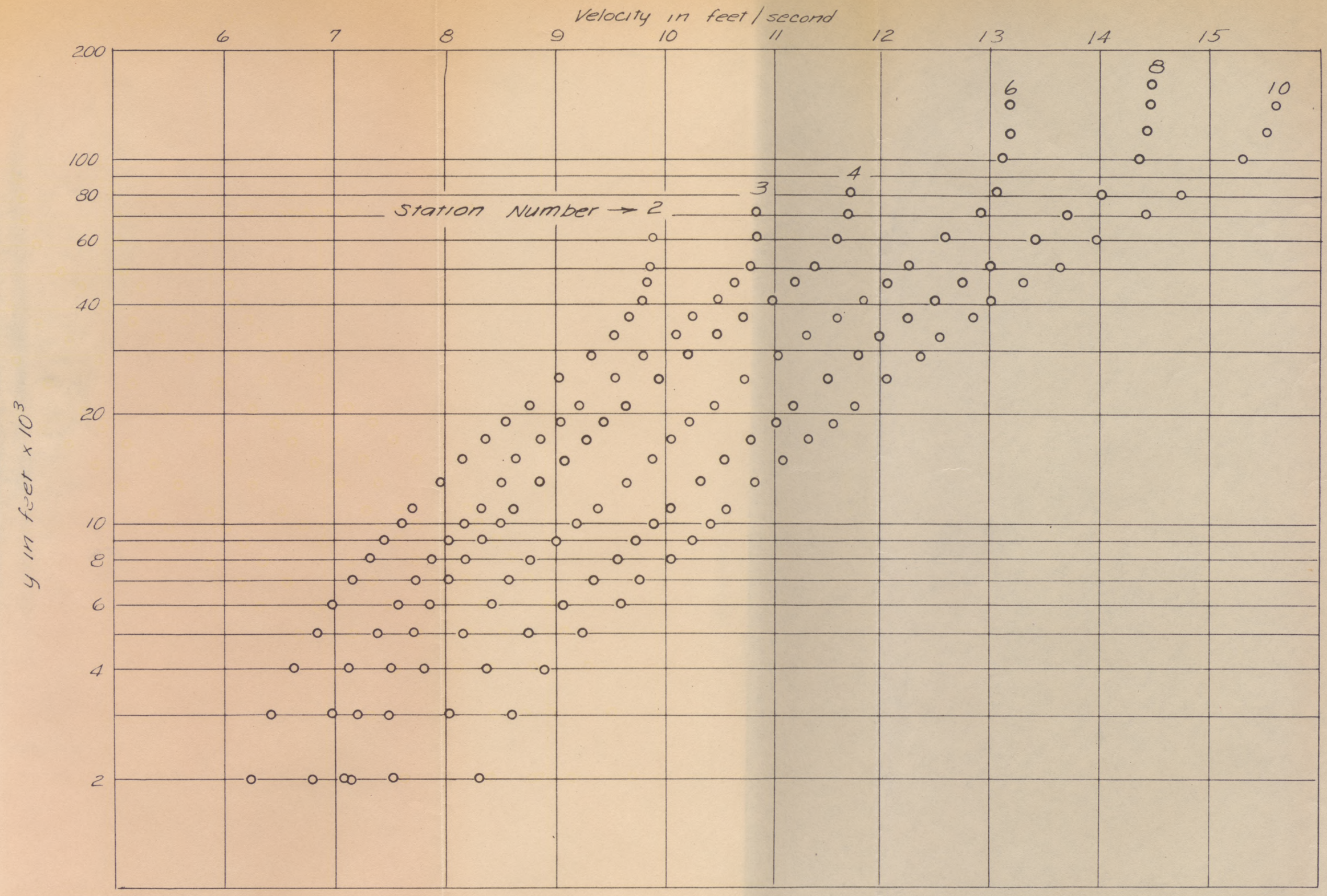


Figure 17. Velocity Profiles, Screen Boundary, 60° Slope, 3.65 cfs/ft





Figure 18 (a). Water Surface, Screen Boundary,  
20° Slope, 1.22 csf/ft.



Figure 18 (b). Water Surface, Screen Boundary,  
20° Slope, 2.98 cfs/ft.

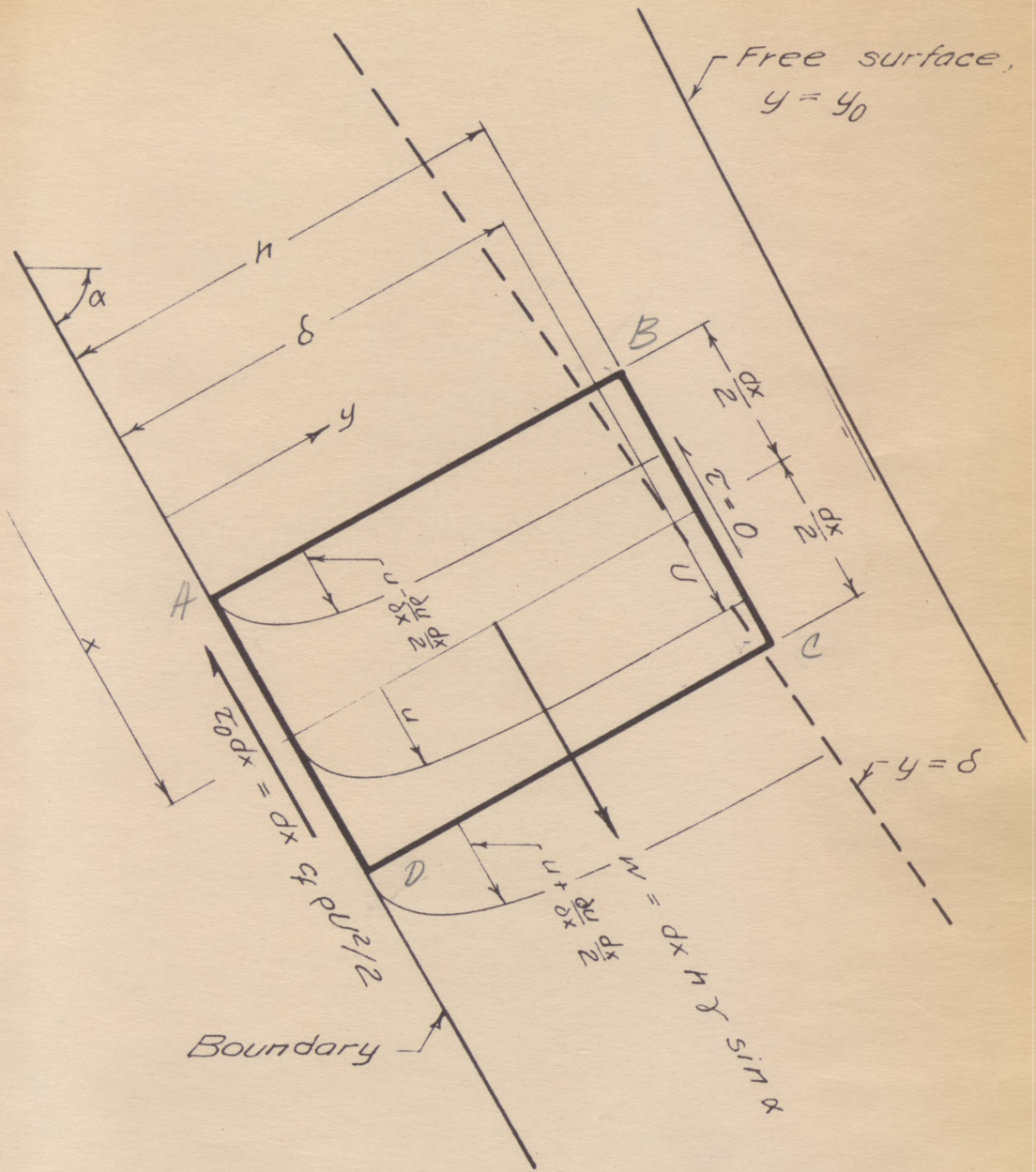
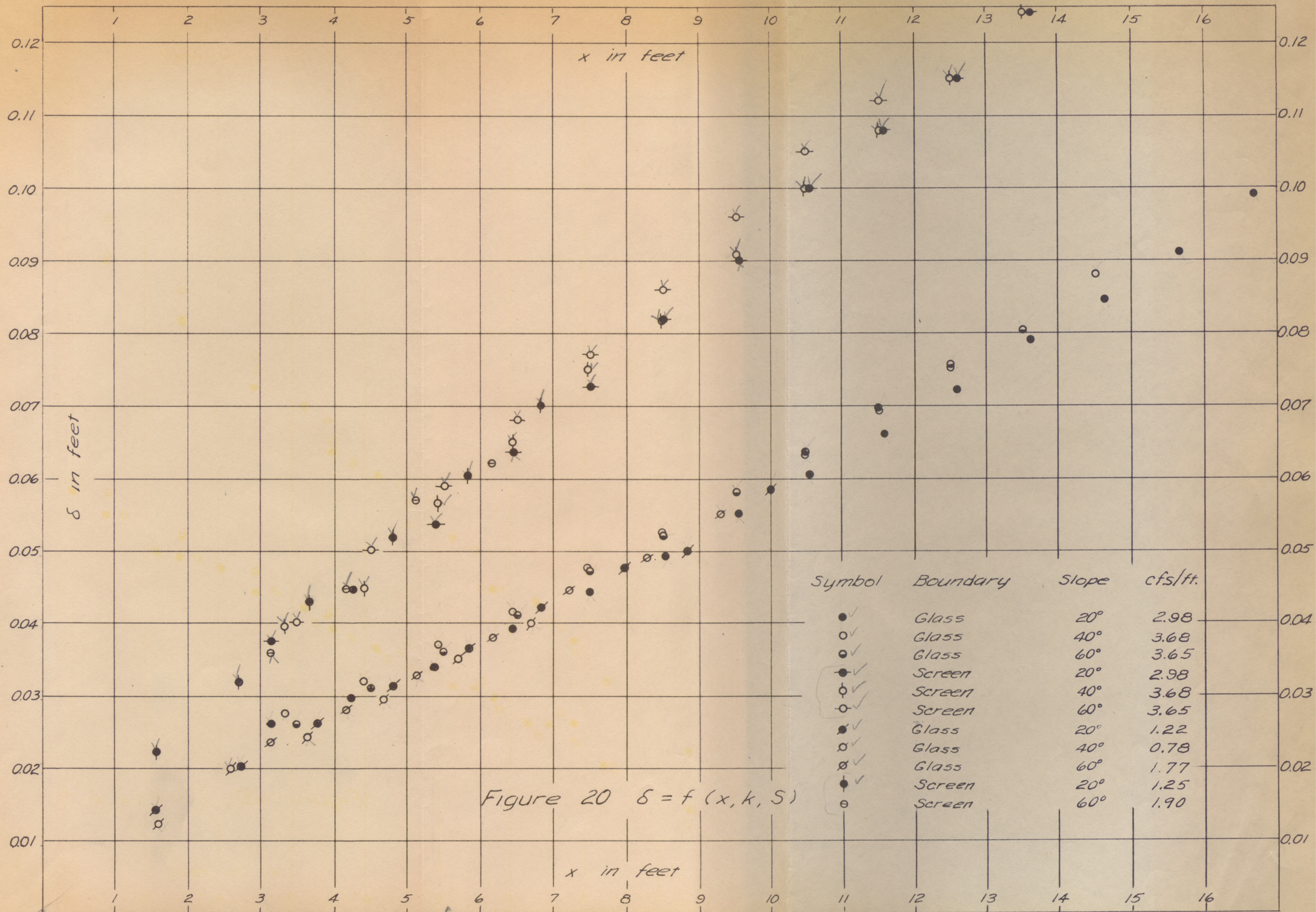


Figure 19. Definition Sketch for Application of Momentum Principle.



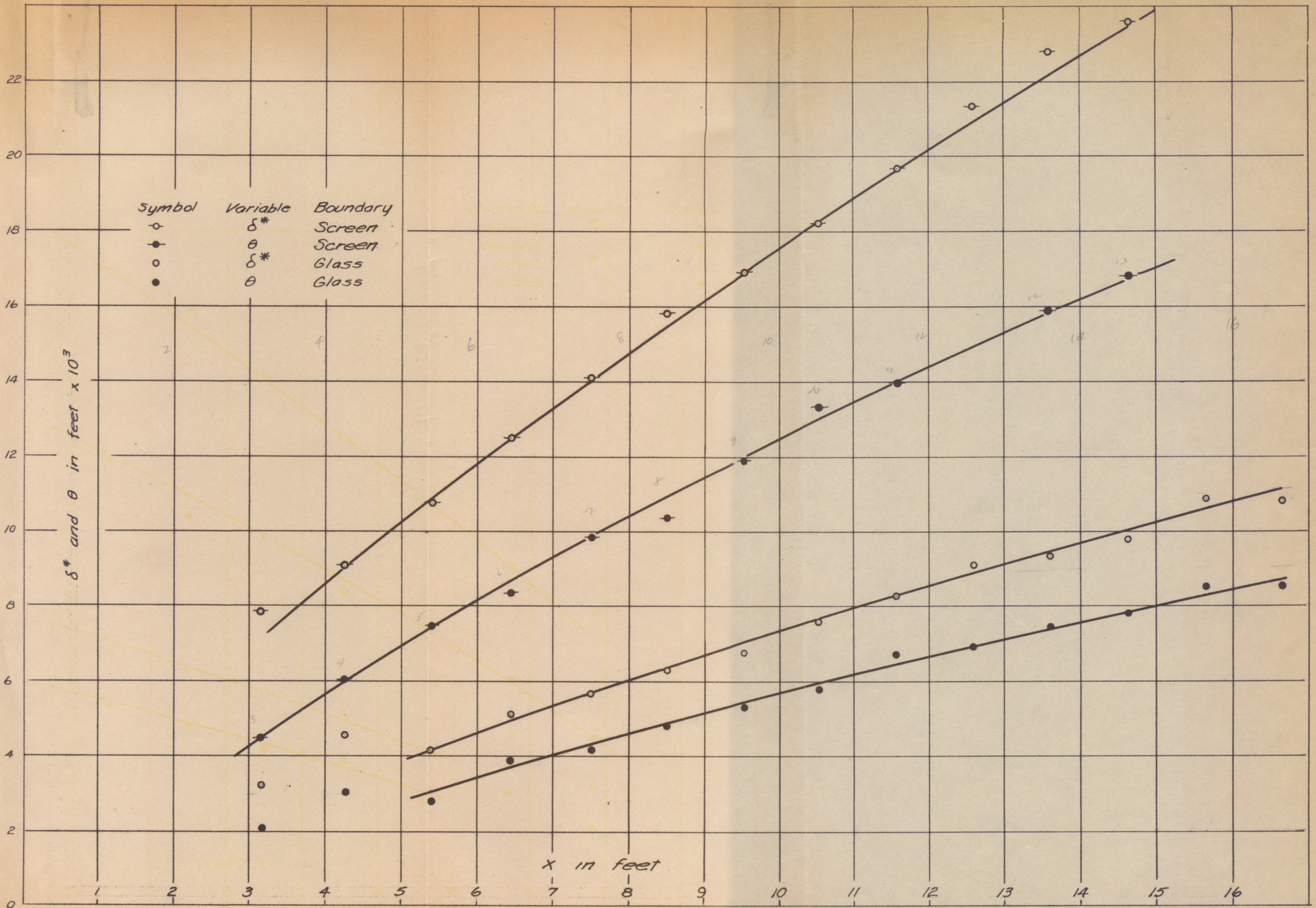


Figure 21.  $\delta^*$  and  $\theta$  vs. x, k on 20° Slope

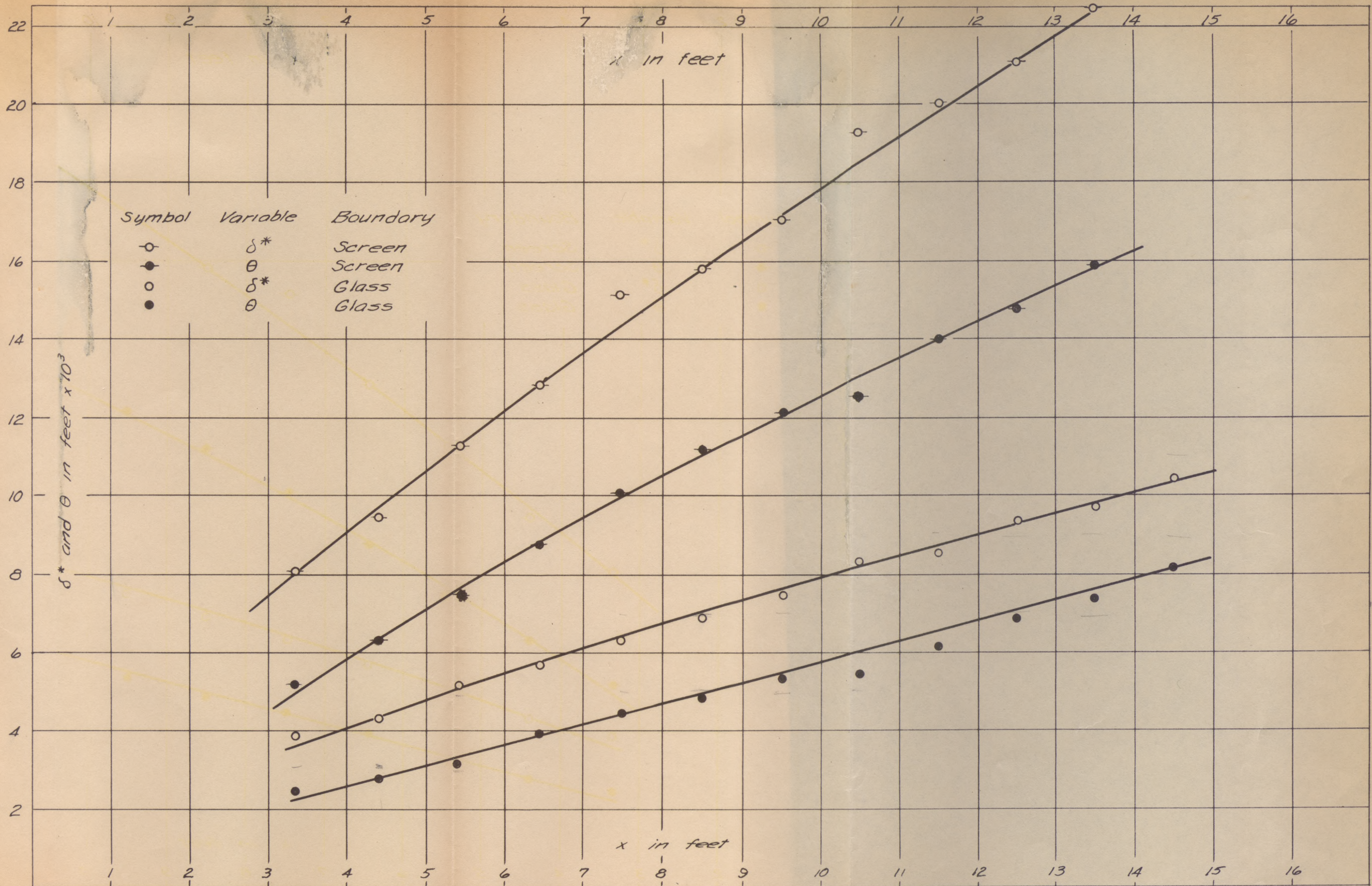


Figure 22.  $\delta^*$  and  $\theta$  vs  $x, k$  on  $40^\circ$  Slope

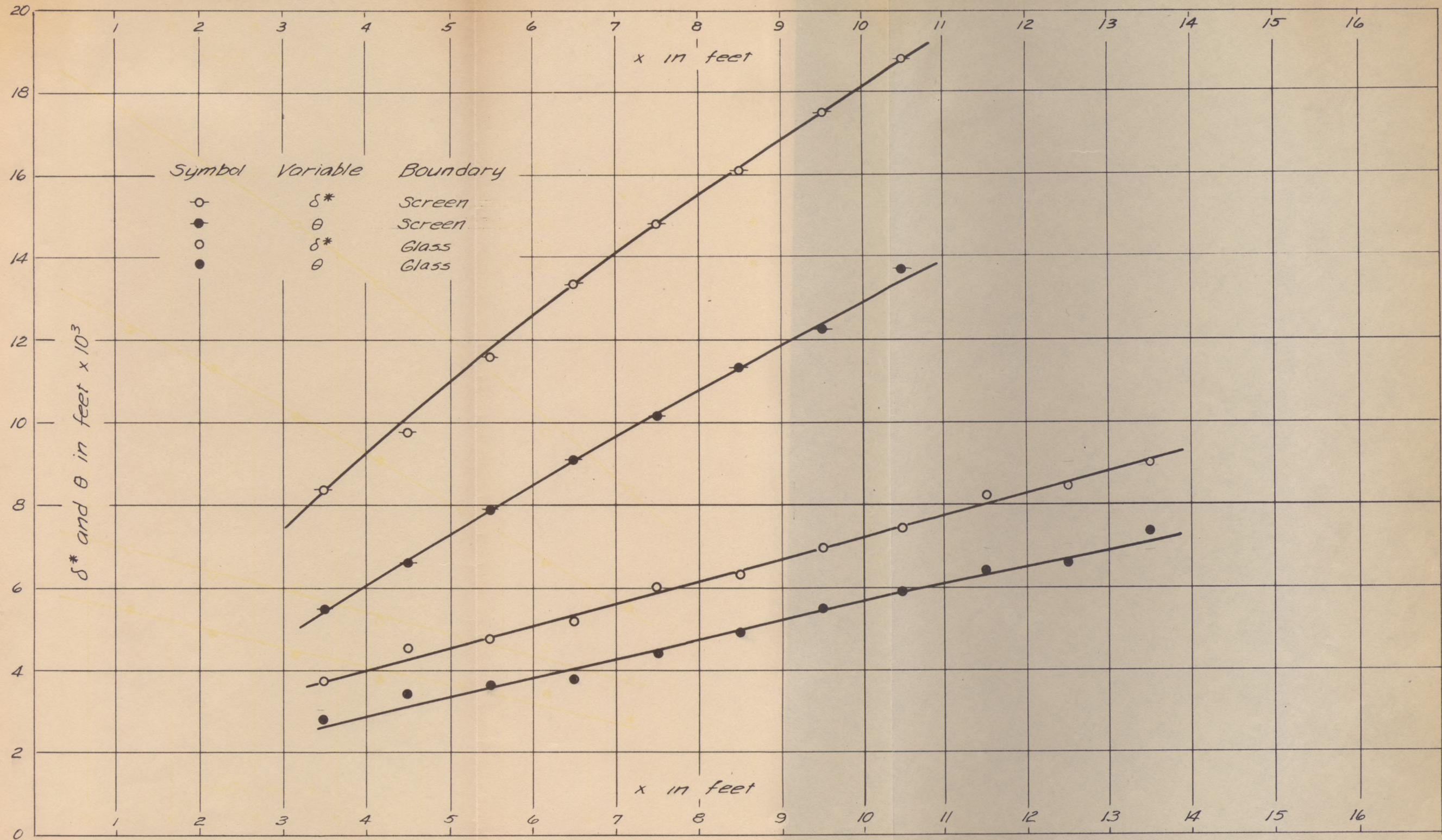


Figure 23.  $\delta^*$  and  $\theta$  vs.  $x, k$  on  $60^\circ$  Slope

$R = Ux/\nu$

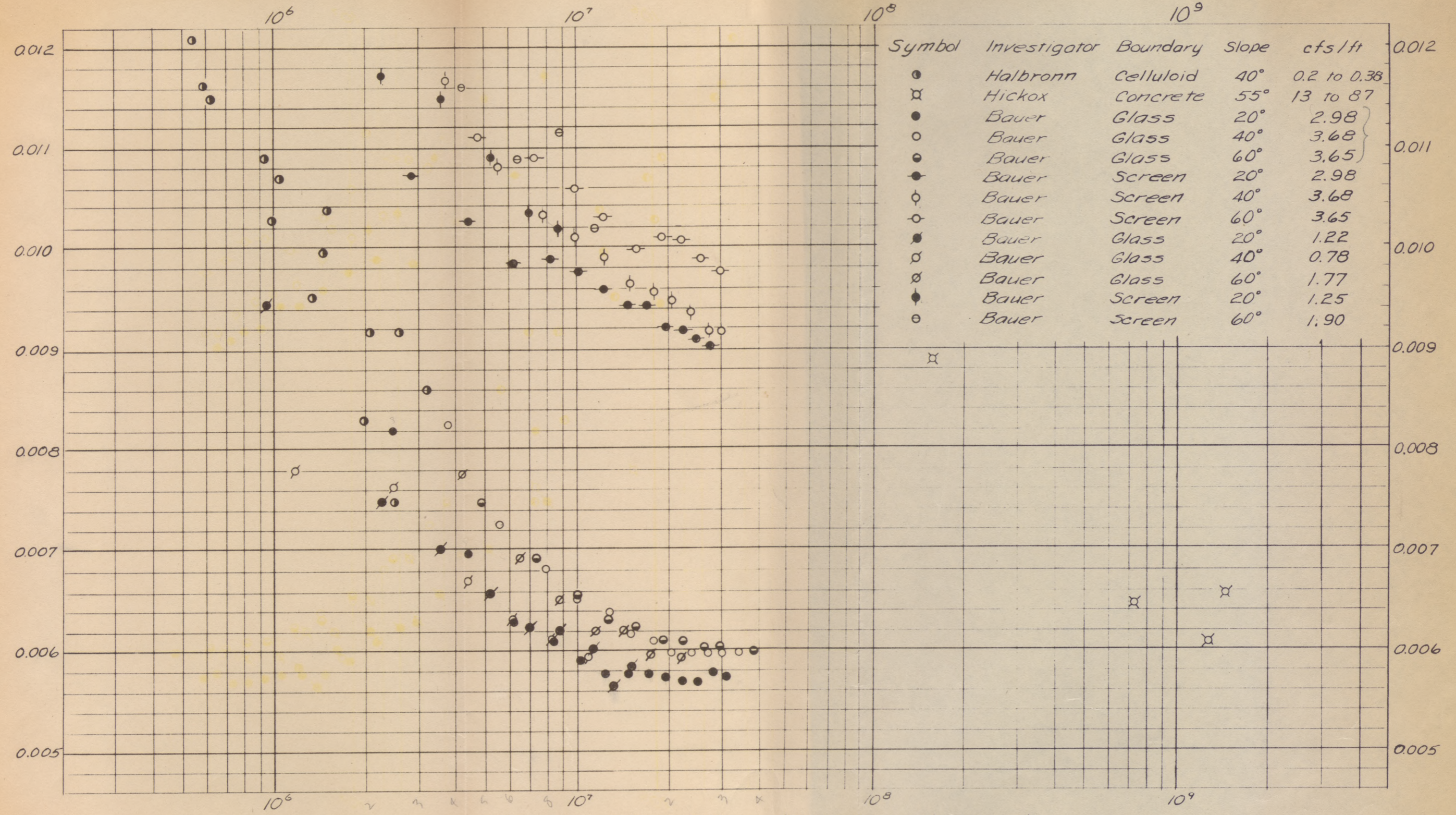


Figure 24.  $\delta/x = f.(Ux/\nu, k/x, S, q)$



$x/k$ , with  $k = 0.009'$  for screen  
and  $k = 0.005'$  for concrete

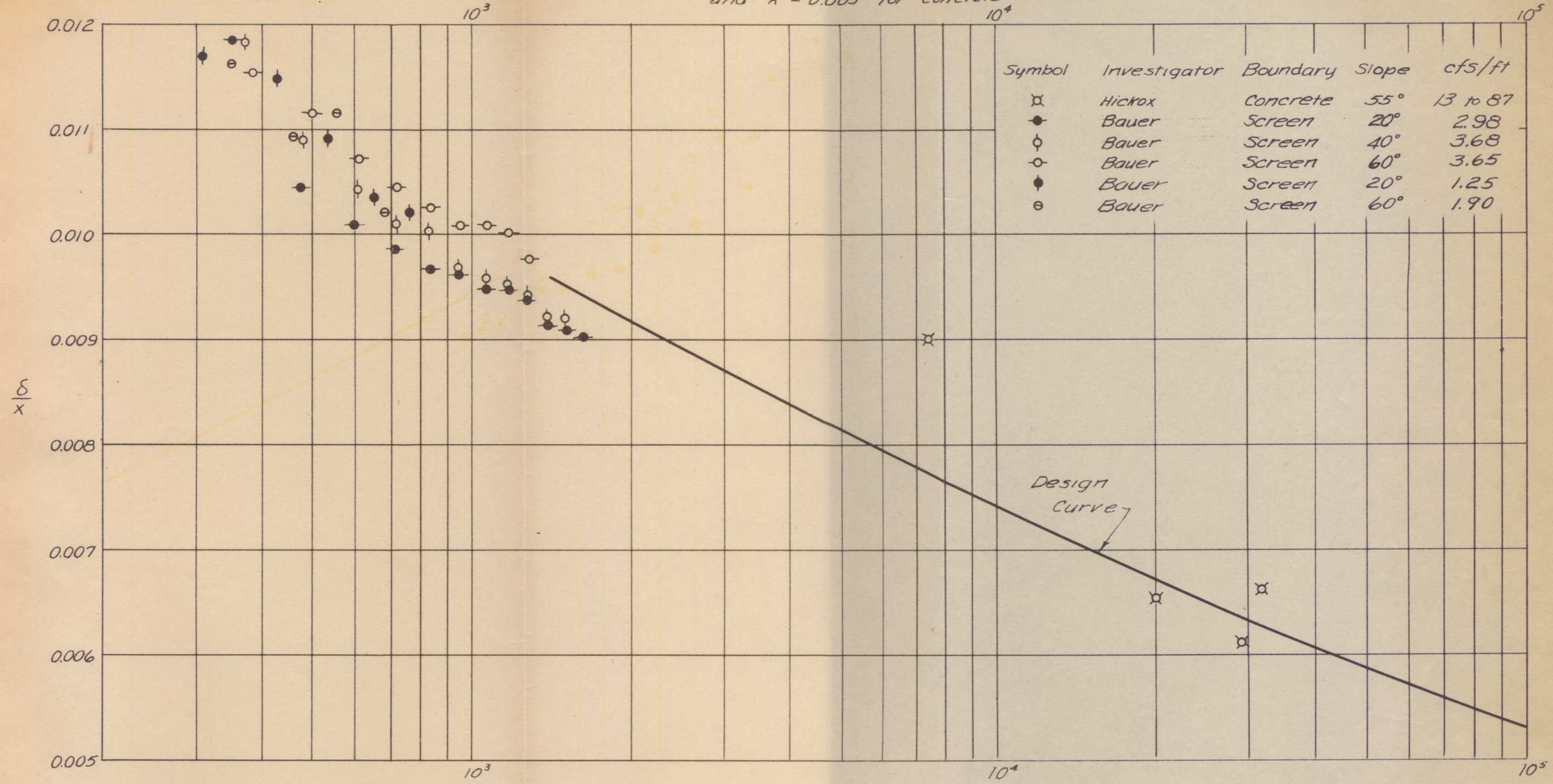


Figure 25.  $\delta/x$  as a function of  $x/k$ .

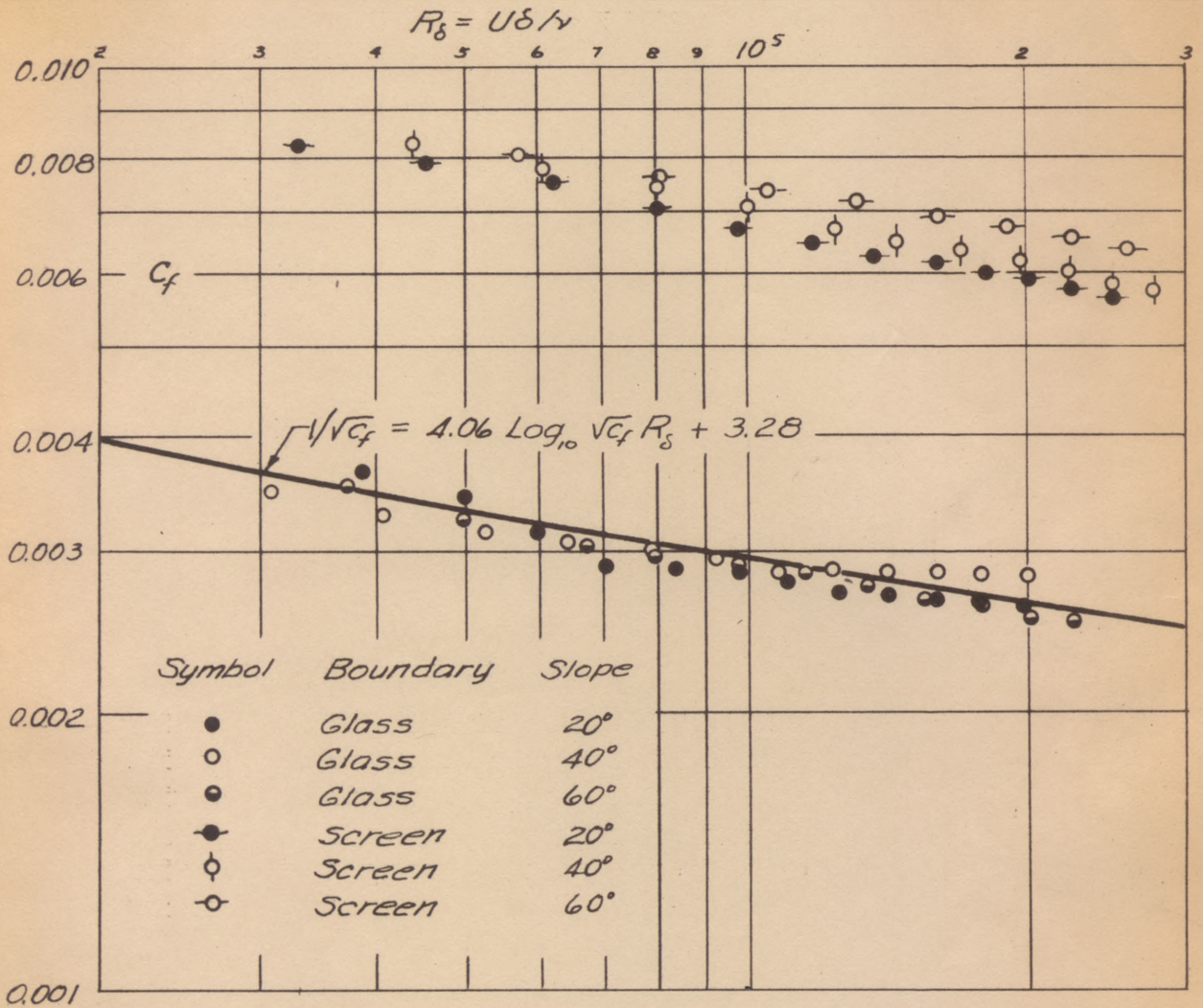


Figure 26.  $c_f$  as a function of  $R_s, k, S$ .

Values of  $\delta/k$ , with  $k$  taken as 0.009'.

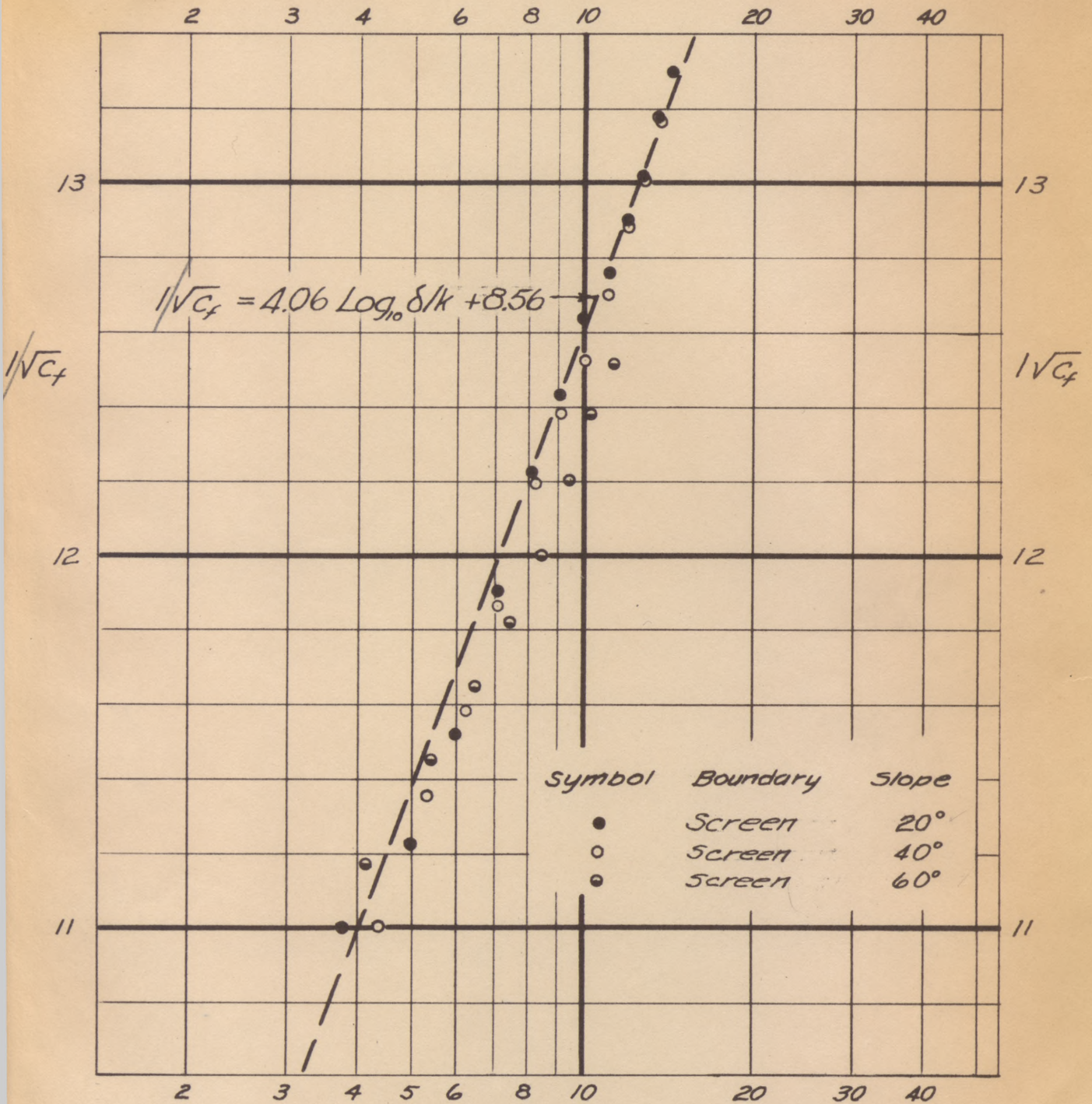


Figure 27.  $c_f$  as a function of  $\delta/k$ .

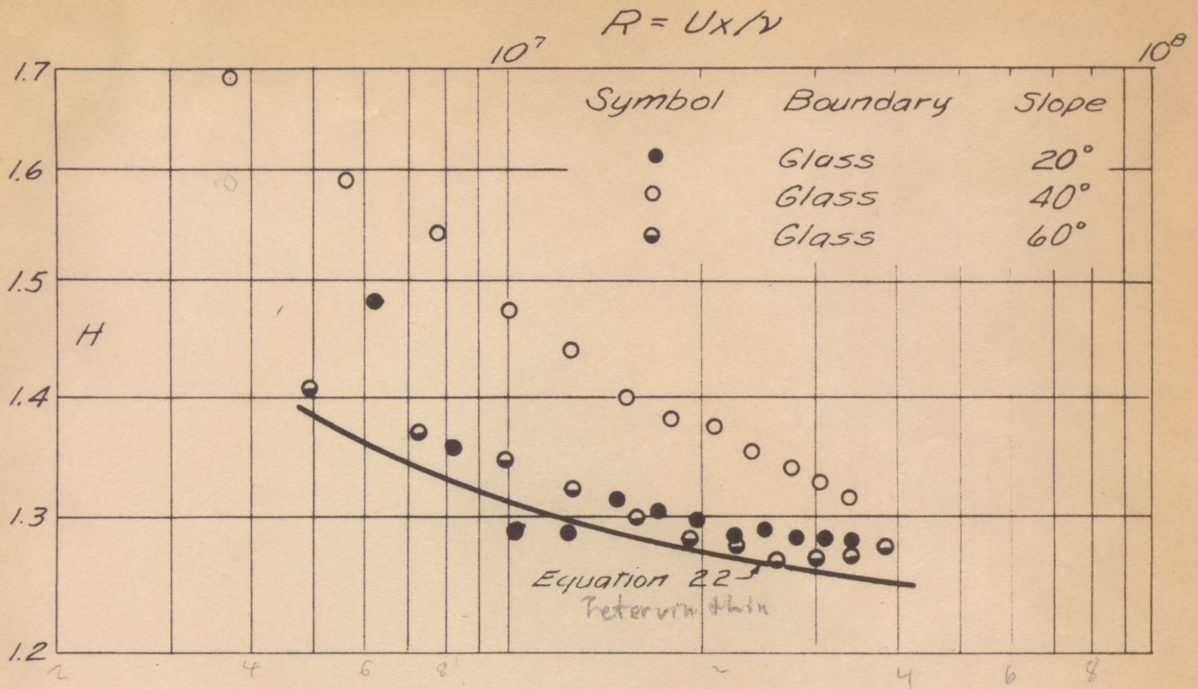


Figure 28.  $H$  as a function of  $R, S$ .

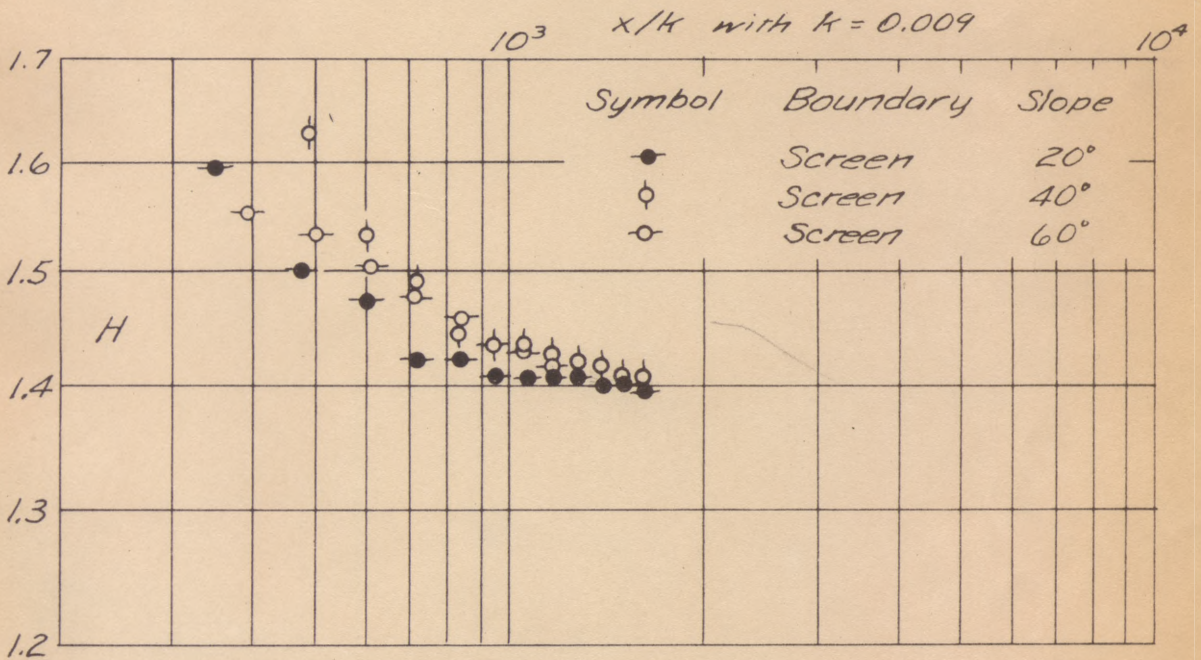


Figure 29.  $H$  as a function of  $x/k, S$ .

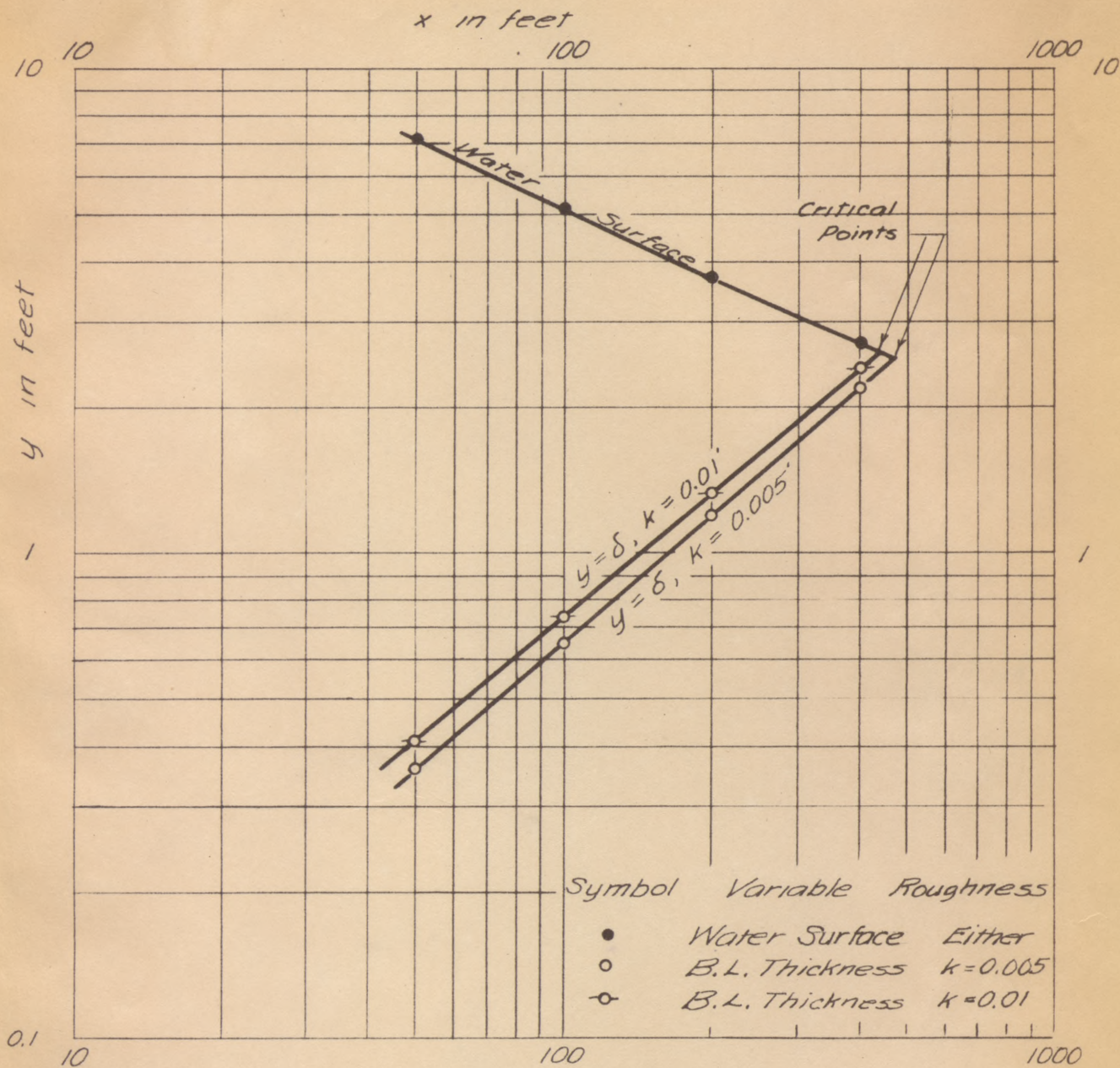


Figure 30. Graphical Solution of Illustrative Example.